

**Inter-Grain Coupling of CuTi-1234 Superconductor
by the Inclusion of Zn Nanoparticles**



By

Ibraheem
(224-FBAS/MSPHY/F13)

Supervisor:

Dr. Muhammad Mumtaz

Assistant Professor
Department of Physics, FBAS,
IIU, Islamabad

**Department of Physics
Faculty of Basic and Applied Sciences
International Islamic University, Islamabad
(2016)**



Accession No TH-16333

K
M. [Signature]

MS
537.623
IBI



Inter-Grain Coupling of CuTl-1234 Superconductor by the Inclusion of Zn Nanoparticles

by:

Ibraheem
(224-FBAS/MSPHY/F13)

This Thesis submitted to Department of Physics International Islamic University,
Islamabad, for the award of degree of MS Physics.

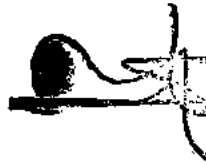


Chairman Department of Physics

3.3.16

International Islamic University, Islamabad.

CHAIRMAN
DEPT. OF PHYSICS
International Islamic University
Islamabad



Dean Faculty of Basic and Applied Sciences

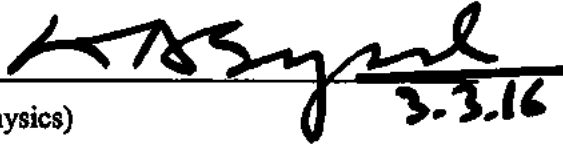
International Islamic University, Islamabad.

Final Approval

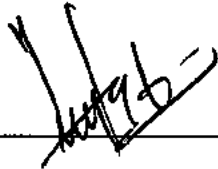
It is certified that the work presented in this thesis entitled “Inter-grain coupling of CuTl-1234 superconductor by the inclusion of Zn nanoparticles” Ibraheem Registration No. 224-FBAS/MSPHY/SF13 fulfills the requirement for the award of degree of MS Physics from Department of Physics, International Islamic University, Islamabad, Pakistan.

Viva Voce Committee

Chairman _____
(Department of Physics)


3.3.16

Supervisor _____



External Examiner _____



Internal Examiner _____



بِسْمِ اللَّهِ الرَّحْمَنِ الرَّحِيمِ

DEDICATED DEDICATED
To
Prophet Muhammad (PBUH),
My Beloved Parents
And
Respected Teachers

Declaration of Originality

I, **Ibraheem** Registration No. 224-FBAS/MSPHY/F13 student of MS Physics (Session 2014-2016), hereby declare that the work presented in the thesis entitled “**Inter-grain coupling of CuTi-1234 superconductor by the inclusion of Zn nanoparticles**” in partial fulfillment of MS degree in Physics from International Islamic University, Islamabad, is my own work and has not been published or submitted as research work or thesis in any form in any other university or institute in Pakistan or abroad.



Ibraheem

(224-FBAS/MSPHY/F13)

Dated: _____

03/03/2016

Forwarding Sheet by Research Supervisor

The thesis entitled “Inter-grain coupling of CuTl-1234 superconductor by the inclusion of Zn nanoparticles” submitted by Ibraheem (Registration No. 224-FBAS/MSPHY/F13) in partial fulfillment of MS degree in Physics has been completed under my guidance and supervision. I am satisfied with the quality of his research work and allow him to submit this thesis for further process to graduate with Master of Science degree from Department of Physics, as per International Islamic University, Islamabad rules and regulations.


Dr. Muhammad Mumtaz

Assistant Professor
Department of Physics,
International Islamic University,
Islamabad

Dated: 03/03/2016

Acknowledgement

I have no words to express my deepest sense of gratitude and numerous thanks to **Almighty Allah**, who enabled me to complete this study and with innumerable blessings for the **Holy Prophet Muhammad (PBUH)** who is forever a torch of guidance and knowledge for the whole humanity. I would like to thank my supervisors **Dr. Muhammad Mumtaz**, Firstly for taking me on as a student and then for providing support, advice for letting me develop my own ideas, and for helping me make it to the end. I would like to pay lots of appreciation to all my teachers, especially **Dr. Kashif Nadeem** who blessed me with knowledge and guidance. My journey wouldn't have been the same without the lab fellows for all the conversations that we had over the year, they always made me smile when the lab days just weren't going right. I appreciate the services of all my senior research colleagues **Irfan Qasim, Liaqat Ali, Waqee-ur-Rehman, Syed Qamar Abbas, Abdul Qahar (IT student)** and especially **Abdul Jabar Bhutta** for being very supportive and co-operative all throughout my research work. I also pay special thanks to my lab fellow **Muhammad Waqas Rabbani, Shehzad Ahmed** and **Irfan Ali** for being helpful in all my research work. My humble and heartfelt gratitude is reserved for my beloved Parents, brother and sisters. Without their prayers and encouragement the completion of this task would have been a dream.

Ibraheem

Table of contents

Chapter: 1.....	6
Introduction.....	6
1.1 Superconductivity	6
1.2 Fundamental properties of superconductors	6
1.2.1 Critical temperature (T_c).....	6
1.2.2 Critical magnetic field (H_c)	7
1.2.3 Critical current density (J_c).....	7
1.2.4 Correlation of three critical parameters	7
1.3 Types of superconductors	8
1.3.1 Type-I superconductors	8
1.3.2 Type-II superconductors.....	9
1.3.3 Intermediate state.....	10
1.4 Theoretical development of superconductivity.....	10
1.4.1 London theory.....	10
1.4.2 London penetration depth in superconductor	11
1.4.3 BCS theory	11
1.4.4 Josephson effect.....	12
1.4.5 Isotopic effect.....	13
1.4.6 Persistent current	13
1.5 CuTI- based superconductors.....	13
1.6 Applications of superconductivity	14
1.7 Nobel prizes in the field of superconductivity	15
1.8 Crystallites and inter-grain connectivity	15
1.8.1 Grain-boundary (GB)	15
1.8.2 Tilt, twist and twin boundaries	17
1.8.3 Role of grain boundaries.....	18
1.9 Nanotechnology	18
1.9.1 Nano-based materials	19

1.9.2	Classification of nano-materials	19
1.9.2.1	Zero-dimensional nano materials	20
1.9.2.2	One-dimensional nano-materials.....	20
1.9.2.3	Two-dimensional nano materials	20
1.9.3	Nanoparticles	20
1.9.4	Applications of Zinc nanoparticles.....	20
1.10	References.....	22
	Chapter 2.....	25
	Literature Review.....	25
2.1	References.....	31
	Chapter 3.....	33
	Experimental techniques.....	33
3.1	Synthesis of high temperature of superconductors	33
3.2	Synthesis of $\text{Cu}_{0.5}\text{Tl}_{0.5}\text{Ba}_2\text{Ca}_3\text{Cu}_4\text{O}_{12-\delta}$ precursors.....	33
3.3	Methods to synthesize nano-structured materials	34
3.4	Sol-gel technique	35
3.5	Steps to synthesize Zn added $\text{Cu}_{0.5}\text{Tl}_{0.5}\text{Ba}_2\text{Ca}_3\text{Cu}_4\text{O}_{12-\delta}$ precursor	36
3.6	Characterization technique.....	37
3.6.1	X-Ray diffraction (XRD) techniques	37
3.6.2	X-Ray diffraction in material science.....	37
3.6.2.1	Bragg's law and X-ray diffraction	37
3.6.3	Laue method	39
3.6.4	Rotating crystal method.....	39
3.6.5	Powder diffraction method	40
3.6.6	Debye Scherrer equation	40
3.7	Scanning electron microscopy (SEM)	40
3.7.1	Background of electron microscopy.....	40
3.7.2	Operation	41
3.7.3	Secondary electron images	41
3.7.4	Back scattered electron images.....	42

3.7.5 Auger electrons	42
3.8 Resistivity measurement	42
3.9 Fourier transform infrared (FTIR) spectroscopy	43
3.9.1 Michelson interferometer	44
3.9.2 Sources of infrared light	44
3.9.3 Detectors	44
3.9.4 Moving mirrors.....	44
3.10 References.....	45
Chapter 4.....	47
Results and discussions.....	47
4.1 Introduction.....	47
4.2 XRD analysis	47
4.3 SEM images	49
4.4 FTIR spectroscopy	51
4.5 Resistivity measurements.....	53
4.6 AC-susceptibility measurements	54
4.7 Conclusion	56
4.8 References.....	57

List of figures

Fig. 1.1: Schematic diagram of zero resistivity and diamagnetism	6
Fig. 1.2: Critical surface diagram of superconducting parameters	7
Fig. 1.3: Schematic figure of Type-I superconductor in applied magnetic field	8
Fig. 1.4: Type-II superconductors in applied magnetic field	9
Fig. 1.5: Formation of Cooper pair in positive lattice	12
Fig. 1.6: Josephson junction between two superconductors	13
Fig. 1.7: Structural diagram CuTl-1223 and CuTl-1234 superconductor	14
Fig. 1.8: Grain boundaries of polycrystalline material (microscopic view)	16
Fig. 1.9: Disturbance in atomic packing at the grain boundary	17
Fig. 1.10: View of tilt, twist and twin boundaries	17
Fig. 1.11: Nanoscience with other disciplines of science	19
Fig. 3.1: Flow chart for synthesis of $\text{Cu}_{0.5}\text{Ba}_2\text{Ca}_3\text{Cu}_4\text{O}_{12-\delta}$ precursor	34
Fig. 3.2: Schematic diagram of Sol-gel process	35
Fig. 3.3: Schematic flow chart of synthesis of Zn nanoparticles/CuTl-1234 nanoparticles superconductor composites.	36
Fig. 3.4: Diffraction of X-rays from crystal planes	38
Fig. 3.5: Schematic diagram of Laue method	39
Fig. 3.6: Rotating crystal method for fixed X-ray wavelength	39
Fig. 3.7: Schematic diagram of SEM	41
Fig. 3.8: Secondary electron view, backscattered electron and auger electron ejection	42
Fig. 3.9: Four probe technique for resistivity measurement	43
Fig. 4.1: XRD pattern of (Zn) nanoparticles	48
Fig. 4.2: XRD patterns of (Zn) _x /CuTl-1234 composites with x = 0 and 3.0 wt. %	49
Fig. 4.3: SEMs of (Zn) _x /CuTl-1234 composites with (a).x = 0, (b).x= 0.6 and (c). x = 1.8 wt. %	50
Fig. 4.4: FTIR spectra of (Zn) _x /CuTl-1234 composites with x = 0, 0.6, 1.2, 1.8, 2.4 and 3.0 wt. %	52
Fig. 4.5: Temperature dependence of resistivity measurements of (Zn) _x /CuTl-1234 composites with x = 0, 0.6, 1.2, 1.8, 2.4 and 3.0 wt. %	53
Fig. 4.6: AC susceptibility of (Zn) _x /CuTl-1234 composites with x = 0, 0.6, 1.2, 1.8, 2.4 and 3.0 wt. %	54

Abstract

We synthesized $(Zn)_x/(Cu_{0.5}Tl_{0.5})Ba_2Ca_3Cu_4O_{12-\delta}$ $\{(Zn)_x/CuTl-1234\}$; ($x = 0\sim 3$ wt. %) nanoparticles-superconductor composites by solid-state reaction technique and examined the effects of zinc (Zn) nanoparticles on structural and superconducting properties of CuTl-1234 phase. Unaltered crystal structure of host CuTl-1234 phase confirmed the existence of Zn nanoparticles at the inter-crystallite sites. We observed an improvement in grains size and inter-grains connectivity by healing up the voids after incorporation of Zn nanoparticles in CuTl-1234 superconductor. The superconducting properties of $(Zn)_x/CuTl-1234$ composites were suppressed for all Zn nanoparticles concentrations. Suppression of zero resistivity critical temperature $\{T_c(0)\}$ and variation in normal state resistivity $\{\rho_{300K}(\Omega\text{-cm})\}$ was attributed to reduction of superconducting volume fractions and enhanced scattering cross-section of mobile carriers across non-superconducting "Zn" nanoparticles at the grain boundaries.

Chapter: 1

Introduction

This chapter includes some basic terms related to superconductivity, historical review and important applications of superconductors. Similarly, some of the basic theoretical and experimental facts are also given, which are necessary for the explanation of superconductivity phenomenon.

1.1 Superconductivity

Superconductors are those materials whose resistivity approaches to zero at specific temperature and become perfect diamagnetic in which the magnetic field lines are repelled from the interior of superconducting material. In conventional prospective, superconductivity is a phenomenon in which resistivity of the material vanishes at a certain temperature called critical temperature " T_c " [1]. Zero resistivity and perfect diamagnetism of superconducting materials are shown in Fig. 1.1.

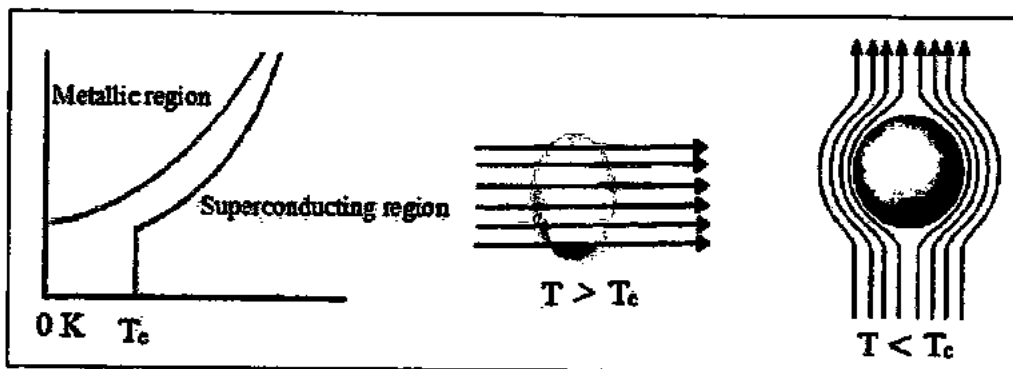


Fig. 1.1: Schematic diagram of zero resistivity and diamagnetism [2].

1.2 Fundamental properties of superconductors

1.2.1 Critical temperature (T_c)

The temperature at which resistivity of a material falls down to zero is called critical temperature " T_c ". Before 1986 the highest " T_c " was about 23 K. In 1986, high temperature superconductors were discovered. Materials having " T_c " greater than 77 K have got special attention because they can be sustained in superconducting phase with liquid nitrogen. In ceramics, $\text{YBa}_2\text{Cu}_3\text{O}_7$ have " T_c " about 92 K [3], and $\text{HgBa}_2\text{Ca}_2\text{Cu}_3$ have " T_c " about 135 K [4].

1.2.2 Critical magnetic field (H_c)

When the superconducting state of the materials transform to normal state at a given magnetic field, this extreme value of magnetic field is known as critical magnetic field " H_c ". As soon as the field exceeds " H_c ", the specimen reverse back to normal conducting state. The value of " H_c " determines the minimum strength of the magnetic field that destroys superconductivity at temperature $T < T_c$.

1.2.3 Critical current density (J_c)

Critical current density " J_c " is the extreme value of current per unit area that a superconductor can transport without destroying the superconducting state. Above " J_c ", the superconducting state of the material vanishes and it goes to normal state. Also " J_c " is temperature dependent property i.e. a superconductor contains more current if its temperature is below " T_c ". Critical current of superconductor for practical use is up to 1000 A/mm^2 .

1.2.4 Correlation of three critical parameters

The three superconducting parameters which are discussed above are strongly inter-related to each other. The main condition for above three parameters i.e. (magnetic field, temperature and current density) is to remain below the critical values. The relationship for these critical parameters is shown in Fig. 1.2. The plot gives the critical surface and explain how the critical parameters are enhanced. In other words, we can say that the material is superconductor inside the surface while it will be normal conductor for outside this surface.

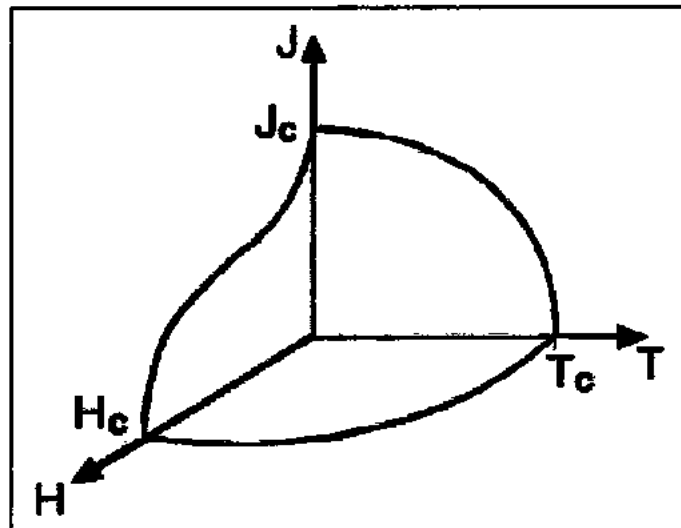


Fig. 1.2: Critical surface diagram of superconducting parameters.

1.3 Types of superconductors

Superconductors are generally classified into two different categories based on their behavior with applied magnetic field [5].

1.3.1 Type-I superconductors

These superconductors are mostly single elements like mercury and lead. They also repel all the applied external magnetic field to become perfect diamagnetic in their superconducting state. Behavior of type-I superconducting materials in applied magnetic field is shown in Fig.1.3. During the superconducting state there is no magnetic field penetration inside the superconductor, which implies the perfect diamagnetism. Type-I superconductors are low temperature superconductors because they are synthesized at low temperature and they are generally known as soft superconductors.

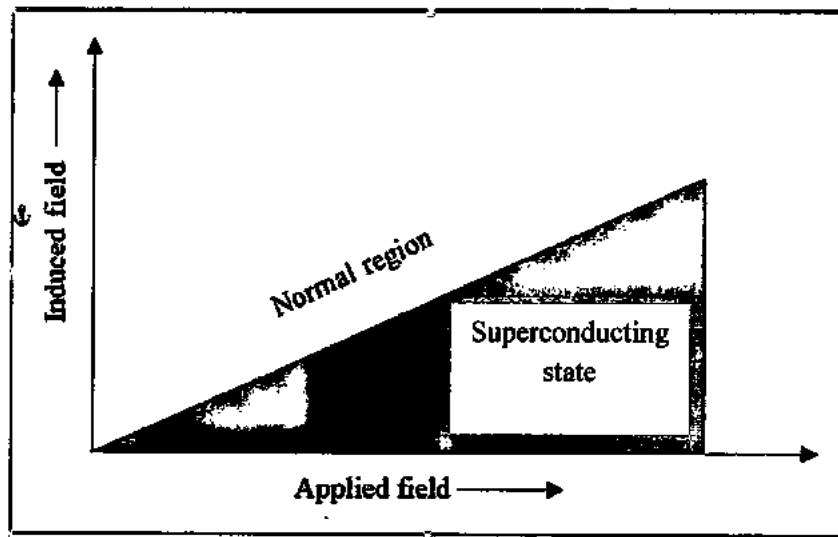


Fig. 1.3: Schematic figure of type-I superconductor in applied magnetic field [6].

List of some known type-I superconductors along with the critical transition temperature (known as T_c) is given Table 1.1. Surprisingly, copper, silver and gold, which are the best metallic conductors are not superconductors. Type-I classification of superconductors is principally included metals and metalloids that demonstrate some conductivity at ordinary room temperature.

Table 1.1: Critical temperature of different elements.

Elements	Symbols	T_c (K)	T_c ($^{\circ}$ C)	T_c ($^{\circ}$ F)
Cadmium	Cd	0.52	-273	-459
Aluminium	Al	1.75	-271	-457
Berullium	Be	0.03	-273	-460
Gallium	Ga	1.08	-272	-458
Mercury	Hg	4.15	-269	-452
Indium	In	3.41	-270	-454
Lead	Pb	7.2	-266	-477

1.3.2 Type-II superconductors

Type-II superconductors include high temperature ceramic superconductors e.g. YBCO, TBCCO and BSCCO. Fig. 1.4 shows the behavior of type-II superconducting materials in applied magnetic field. Two critical fields exist in type-II superconductors represented as H_{c1} (lower critical magnetic field) and H_{c2} (upper critical magnetic field). Before H_{c1} , externally applied magnetic field is completely expelled and material shows completely diamagnetic behavior. In the region between H_{c1} and H_{c2} magnetic field partially penetrate into the material and it exhibit partially diamagnetic behavior. This state between H_{c1} and H_{c2} in high temperature superconductors is termed as vortex state or mixed state. After H_{c2} magnetic field completely penetrate into the material and it behaves as a paramagnetic material and show small magnetization [7].

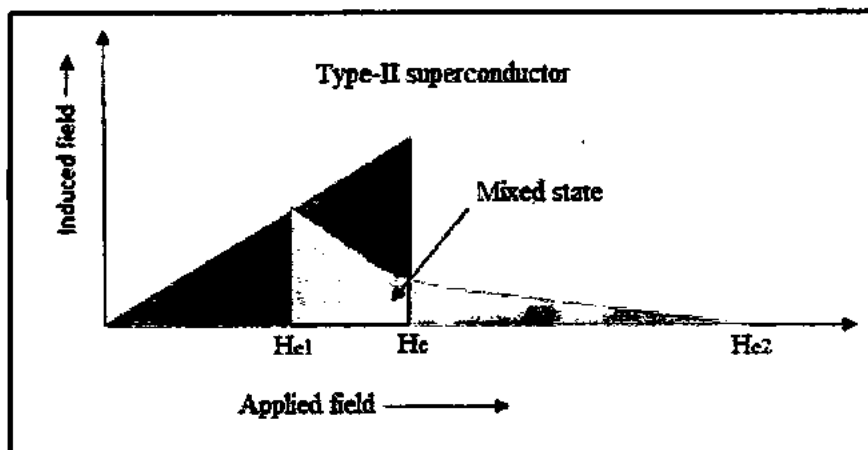


Fig. 1.4: Type-II superconductors in applied magnetic field [8].

1.3.3 Intermediate state

The hybrid of both normal and superconducting state is called intermediate state. Whenever the external magnetic field start increasing, the sample will cross the superconducting region, i.e. $H < H_{C1}$. It means that number density will increase and the vortices will be created. Magnetic field can pass through these vortex and become non superconducting region. The sample is in superconducting state for outside the vortices while for inside region, the material is in normal state. The vortex number density is maximum in the region where H tends to H_{C2} . To enhance the superconducting transport properties, these states can be filled with the help of different techniques [8].

1.4 Theoretical development of superconductivity

Superconductivity is a special characteristics of the materials. Different theories were presented to explain the origin, nature and different properties of superconductors. In 1935, two brothers Fritz and Heinz London presented a theoretical model, which is based upon the two fluid assumptions. The microscopic theory presented by John Bardeen, Leon Neil Cooper and John Robert Schrieffer to explain the exact mechanism of electron motion (BCS theory). BCS theory in its simplest structure is really conflicting to naturally macroscopic view. Superconductivity starts increasing when electrons don't interact destructively with atoms in crystal structure of composites.

1.4.1 London theory

It is clear that the behavior of superconducting material is different from other materials. In order to study the behavior of superconductors in an external electric and magnetic field, this theory follow two fluid models. The total number of electrons which are moving in superconducting materials are divided into two types. The first one is " n_n " represents normal electron density and " n_s " i.e superconducting electron density. For total number density of electrons, we can write;

$$n = n_s + n_n$$

In superconducting state, n_s is dominant while in ordinary conducting materials n_n is dominant.

$T \rightarrow T_c$, $n_n \rightarrow 0$ & $n_s \rightarrow \max$ for $(T \rightarrow T_c)$ and $n_s \rightarrow 0$ & $n_n \rightarrow \max$ as $T \rightarrow T_c$ for $(T \rightarrow T_c)$

Let us consider a superconducting material inserted in both electric and magnetic field. The superconducting electron density will not be affected if both the fields have probably low values. London equation gives us the relation between linear electric and magnetic field [9].

$$\frac{\partial J_s}{\partial t} = \frac{n_s e^2}{m} E, \quad \nabla \times J_s = -\frac{n_s e^2}{mc} B \quad 1.1$$

In above equation " n_s " is the number density " m " is the mass " e " is charge of electron and " E " is the electric field. So the current density for superconducting state is

$$J_s = n_s e v_s. \quad 1.2$$

Where " v_s " is the speed of superconducting electrons.

1.4.2 London penetration depth in superconductor

London penetration depth is theoretical approach to discuss the penetration distance of magnetic field inside superconductor and its exponential decay. It shows the relationship between curl of current density " J " and magnetic field B .

In electrodynamics, the 4th Maxwell equation is

$$\nabla \times B = \mu_0 J_s \quad 1.3$$

This equation is applied to calculate the London penetration depth for superconducting state.

Taking curl of the above equation we get

$$\nabla \times (\nabla \times B) = -\frac{\mu_0 n_s e^2}{m} B = -\frac{1}{\lambda^2} B \quad 1.4$$

In above equation λ_L represents the London penetration depth. Therefore for λ_L we can write

$$\lambda = \left(\frac{m}{\mu_0 n_s e^2}\right)^{1/2} \quad 1.5$$

Because,

$$\nabla \times (\nabla \times B) = \nabla(\nabla \cdot B) - \nabla^2 B$$

While from Maxwell 3rd equation for magnetic monopole, we have

$$(\nabla \cdot B) = 0$$

So,

$$\nabla^2 B = \frac{1}{\lambda^2} B \quad 1.6$$

Using calculus, the 1-D solution of given equation is,

$$B = B_0 e^{-x/\lambda} \quad 1.7$$

Hence we can say that London theory explain the exponential disintegration of external applied field [10].

The value of London penetration depth is ranging from 100 to 1000 Å. It's small value is in agreement of experimentally observed Meissner effect.

1.4.3 BCS theory

This theory explain the characteristics of low temperature superconductor when two electrons form a pair in lattice of superconductor. This theoretical understanding about superconductivity is explained in 1957 by Bardeen, Cooper and Schrieffer. Such theory

represents the conventional pairing of electron is known as Cooper pair. Fig.1.5 shows the electron pair and retardation of lattice parameters.

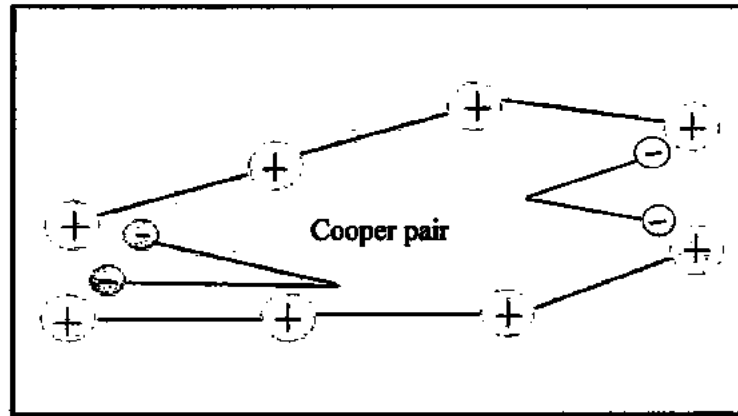


Fig. 1.5: Formation of Cooper pair in positive lattice.

When an electron flows in superconducting material without experience any resistance, this electron is attracted towards positive lattice ion due to coulomb attractive force. This attraction produce vibration in lattice and hence another electron enter in distorted lattice ion. Thus Coulomb repulsive force of these two electrons is overcome by Coulomb attractive force between two electrons. The phonon is emitted during this lattice vibration to decrease the energy of the system and two electrons form a pair known as cooper pair. The energy of cooper pair is smaller than band gap energy and it moves in superconducting material without losing superconductivity. When Cooper pair overcome the band gap energy, superconductivity is reduced and cooper pair break up [11].

1.4.4 Josephson effect

An English Physicist B. D. Josephson in 1962 introduced mathematical expression of current across the weak links. According to Josephson Effect, the super current can achieved in insulator of small thickness when it is sandwiched between two superconductors. This insulator of small thickness is known as Josephson junction and current which is established by external supply is flowing across this junction by removing the external source as shown in Fig. 1.6. This phenomenon is observed by repeated experiments and galvanometer deflect across the junction for all observations. Josephson junction can enhance the superconducting parameters in type-II superconductors [12].

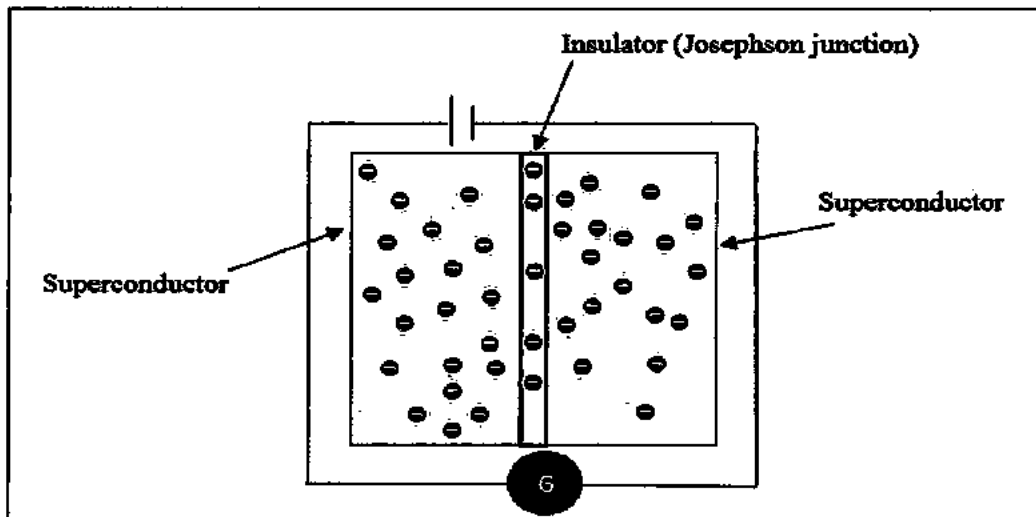


Fig.1.6: Josephson junction between two superconductors.

1.4.5 Isotopic effect

According to Froehlich, the lattice ions and electrons interaction are dependent parameters for superconductivity. He suggested that increasing the number of neutrons (isotopic mass) can produce the superconducting materials of lower critical temperature. Furthermore, electron collision is increased by increasing isotopic mass which produce distortion. Mathematical expression for isotopic mass increase is given as

$$M^a T_c = \text{constant} \quad 1.8$$

Where "a" is fitting constant. BCS theory can be examined by isotopic mass result [13-14].

1.4.6 Persistent current

It is suggested that when a current is established in superconductor, the charges inside the bulk will move without any resistance and hence produce current for long intervals of time. Superconducting electromagnets are used to produce high magnetic field using persistent current. This current was identified by Onnes. It is estimated that the current which is established in superconducting materials will remain for 10^5 years [15].

1.5 CuTl- based superconductors

Sheng and Hermann were first to discover copper thallium based superconductors. These have very prominent uses because of their high " T_c " values. The crystal structure of CuTl-based superconductor is shown in Fig.1.7 which have high coherence length along c-axis, lower superconducting anisotropy and higher critical temperature. Large voids, pores and

weak links in the interior may reduce the performance of these superconductors. Moreover, vortices movement in HTSCs produce resistance, which cause energy dissipation. It is observed that inclusion of metallic and magnetic nanoparticles sometime increase the superconducting parameters up to certain optimum level and then start decreasing [16-19].

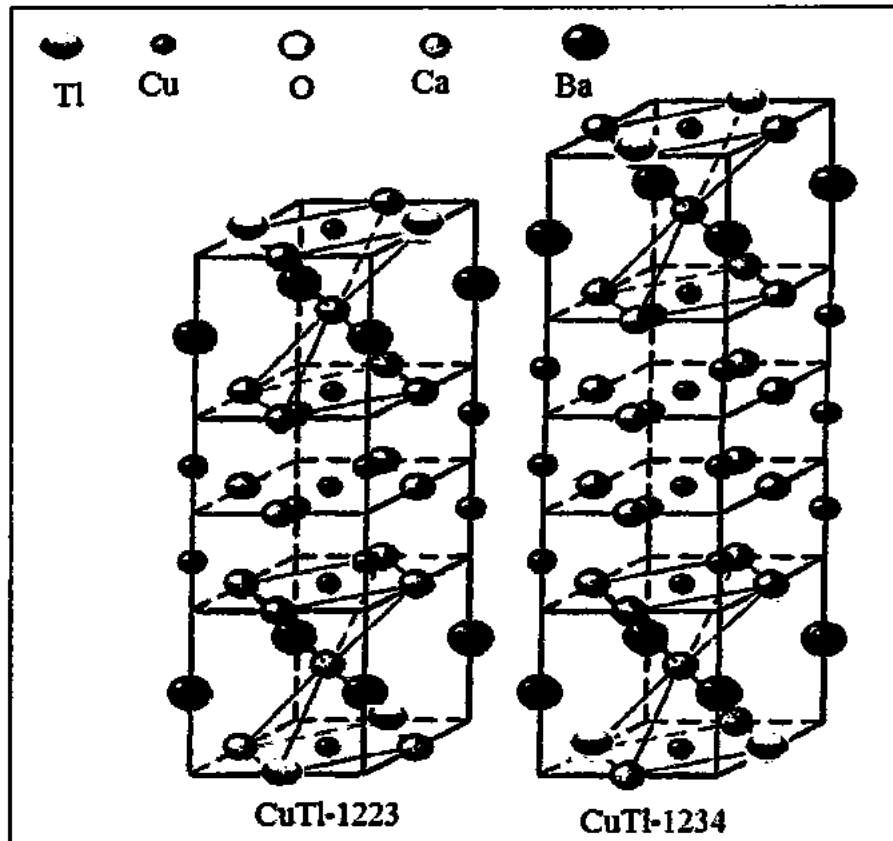


Fig.1.7: Structural diagram of CuTi-1223 and CuTi-1234 superconductor.

1.6 Applications of superconductivity

Superconductors are widely operational in laboratories and expect that it will be used in our cities and homes. The cooling of these materials at a very low temperature is an issue which restrict their uses in daily life. If a superconductor which do not require such cooling is discovered, then all energy problems will be resolved. Some applications of superconductors are dicussed below.

(1) Superconducting quantum interference devices (SQUID), flux detectors and modern computers are the applications based on Josephson effect. Using SQUID device, a very weak magnetic field can be detected.

(2) Superconducting applications of Meissner effect are magnetic levitation trains and magnetic shielding effect. Superconductors can be used to shield out unwanted magnetic flux, as in shaping the magnetic lens system of a scanning electron microscopy.

(3) Direct currents and voltages can be amplified and a signal of very low noise are traced out by using high temperature superconductors.

1.7 Nobel prizes in the field of superconductivity

(1) In 1913, Heike Kammerlingh Onnes won Nobel prize in Physics by studying "properties of matter at low temperature".

(2) Nobel prize in physics of the year of 1972 was given on the title of "BCS-theory" and shared by John Bardeen, Leon N. Cooper and J. Robert Schrieffer.

(3) In 1973, Brian D. Josephson, Ivar Giaever and Leo Esaki shared Nobel prize in Physics on the tunneling phenomenon in superconductors and semiconductors as well as "for his theoretical predictions of the properties of a supercurrent or (Josephson effect)".

(4) Physics Nobel prize of 1987 was given to J. Georg Bednorz and K. Alexander Müller for "discovery of superconducting phenomenon in ceramics materials".

(5) The Nobel prize of 2003 was awarded jointly to Alexei A. Abrikosov, Vitaly L. Ginzburg and Anthony J. Leggett "for pioneering contributions to the theory of superconductors and superfluid.

1.8 Crystallites and inter-grain connectivity

Each surface of any material consists of surface defects, which can cause to suppress the electrical, magnetic and charge carriers properties of materials. These defects are planar defects or grain-boundaries, line-defects or dislocations, point-defects and surface roughness etc. In case of superconducting materials, these defects reduce superconducting parameters and transport properties. Different crystallites of polycrystalline materials are separated in adjacent layers as a result of these surface defects [20].

1.8.1 Grain-boundary (GB)

One of the major surface defect is grain-boundary, which is the interface and empty space between two grains or crystallite and important surface defect from the mechanical point of view. Polycrystalline solid consists of several crystals which are also called crystallite grain. These crystallites or grains are appeared during the cooling process of many compounds. These boundaries appear as a result of uneven growth during crystallizing a solid. Each crystalline material has millions of individual grain boundaries as shown in Fig. 1.8. These boundaries

can be described in terms of dislocation arrays. It is observed that grain boundaries have rapid chemical reaction from the grains. Different nanoparticles occupy these boundary regions in superconducting materials due to their more surface to volume ratio that reduce the weak links and enhance the carrier transport properties. Grain sizes vary from 1 μm to 1 mm [21].

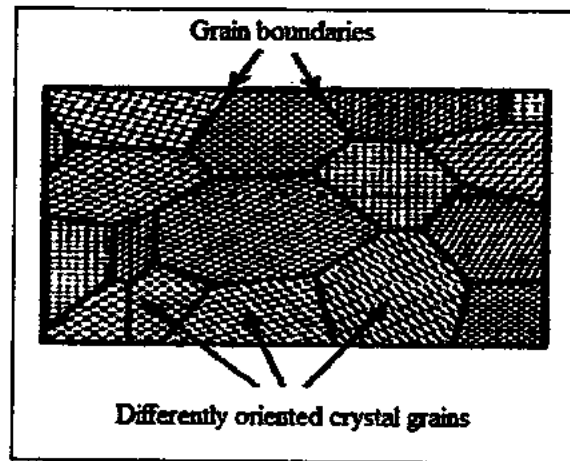


Fig. 1.8: Grain boundaries of polycrystalline material (microscopic view).

Each and every grain has different orientations because there is systematic packing of atoms in any individual grain. The grain-boundary has probably simple configuration for small misorientation between the two grains called a low angle grain-boundary as shown in Fig. 1.9. When more complicated structure is achieved, the misorientation becomes large and known as high angle grain boundary. Configuration of soap bubbles for crystal structure simulation is an example of high angle grain-boundary. So grain boundaries appeared, when two grains meet each other in solid or when there is some disturbance in the atomic packing. Moreover, transition regions of neighboring crystals produce grain boundaries.

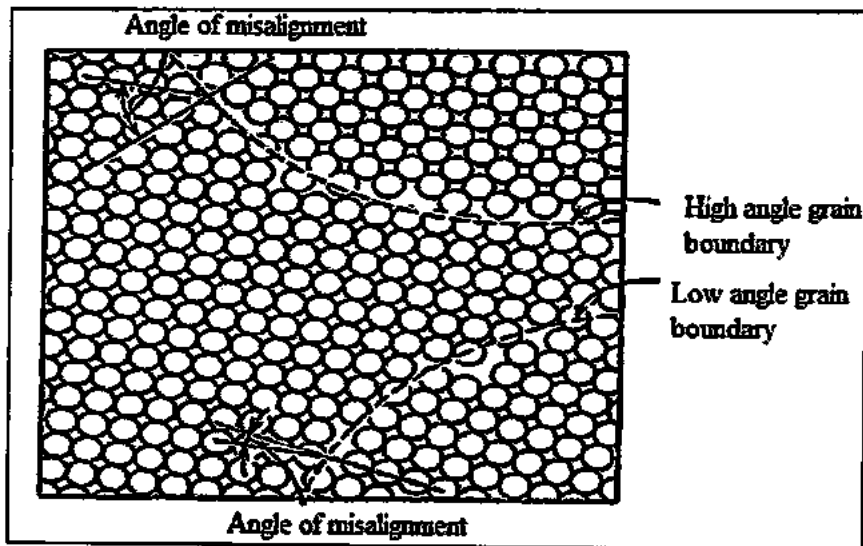


Fig: 1.9: Disturbance in atomic packing at the grain boundary [22].

1.8.2 Tilt, twist and twin boundaries

The tilt boundary is the simplest grain boundary have remarkable configuration of edge dislocations between two crystallite. Rotation axis is parallel to the boundary plane in tilt boundary but in twist boundary, this rotation axis is perpendicular to the boundary plane. Moreover, in twin boundary, the atomic arrangement of one side is the mirror image of that arrangement on the other side as shown in Fig. 1.10. Similarly, shear deformation of bi-crystal materials and annealing heat treatment caused twin boundaries [23].

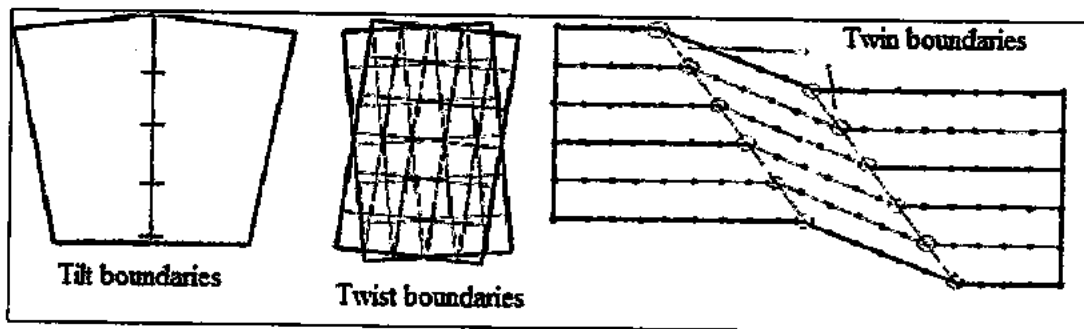


Fig. 1.10: View of tilt, twist and twin boundaries.

Mathematically, the dislocation space "D" for the misorientation " θ " at the boundary is given as,

$$D = \frac{b}{2\sin\left(\frac{\theta}{2}\right)} \approx \frac{b}{\theta} \quad (\text{For very small } \theta) \quad 1.9$$

Here b is the Burger vector. The distance between two dislocations become small when misorientation " θ " start increasing. For large angle " θ " the dislocations are specified by one or two atomic spacing. By intersecting tilt and twist boundaries, we can also generate misorientation but in such a case, the structure of grain boundary may be the sum of edge and screw dislocations [24].

1.8.3 Role of grain boundaries

The role of grain boundaries in plastic deformation of polycrystalline compounds is very important. It is generally accepted that the properties of polycrystalline materials can be controlled by their structure and interfaces especially by grain boundaries. Some basic aspects of grain boundaries are discussed below.

- (1) The grain boundaries are responsible for dislocation movement at lower temperature ($T < 0.5T_m$, where T_m is melting point in Kelvin). These mobile dislocations can stacked together against each grain boundaries and increase the stress concentrations.
- (2) Each grain produce slight deformation in polycrystalline materials where the progression of voids and cracks is not permitted. Thus grains produce the condition of compatibility for neighboring grains. Smaller the grain size, larger will be the total boundary surface area per unit volume. In similar statement, we can say that smaller grain size enhance the work-hardened property of materials for a given deformation.
- (3) At high temperatures the grain boundaries properties are the sites of weakness. As a result, the plastic flow and production of voids at boundaries are appeared.
- (4) At high temperature, the grain boundaries are considered as source and sink for all vacancies. Hence leading to diffusion current in Nabarro Herring creep mechanism.
- (5) In polycrystals, each and every grain has random orientation with respect to one another [25].

1.9 Nanotechnology

An American physisist Richard Feynman delivered a lecture of title "There is plenty of room at the bottom" on 29 December, 1959 at an American physical society. This famous lecture adopted the idea of new science as "nanotechnology" based on nanometer dimensions. The materials whose one dimension is controlled from 1-100 nm range are known as

nanomaterials. These materials show a remarkable changing from bulk materials like high surface to volume ratio, high reactivity and important quantum effects. Fig.1.11 gives the relation of nanotechnology with other fields due to their major physical and chemical properties [26].

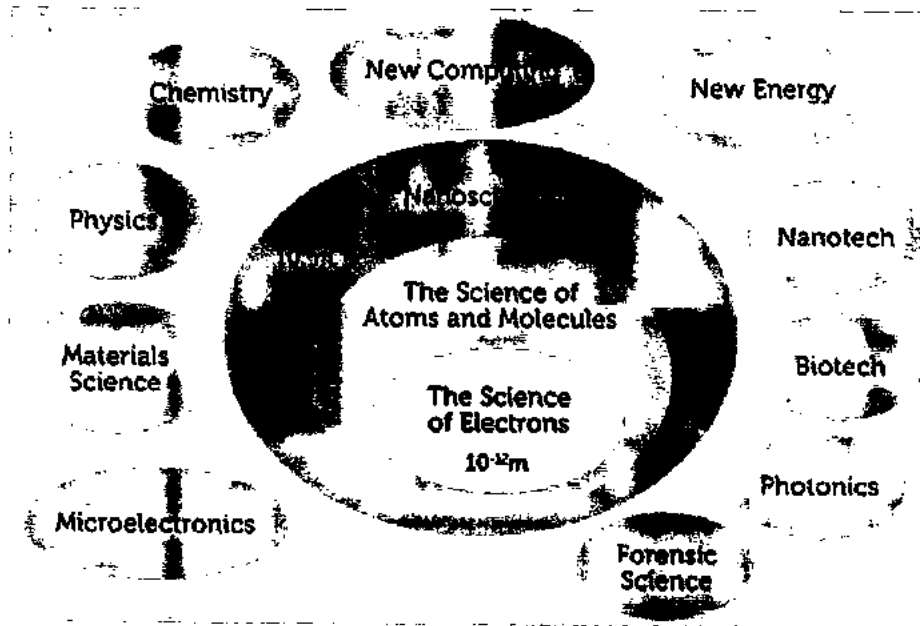


Fig. 1.11: Nanoscience with other disciplines of science.

Nanomaterials transform their properties from macroscale to nanoscale due to their size reduction. For instance, chemically inert materials at normal scale, behave as effective chemical catalyst at nanoscale, insolubles behave as soluble (gold), opaque objects as transparent (copper) and stable materials as combustible (aluminium).

1.9.1 Nano-based materials

Nano-based materials are those materials which have confined dimensions either all or single one less than 100 nanometer or equal to the De- Broglie wavelength. As the size of these materials is 100,000 times smaller than human hair, these materials have remarkable applications in different fields. This technology has broad and useful properties to make the life better and easy due to their unique electrical, optical and magnetic properties [27].

1.9.2 Classification of nano-materials

Nano-materials are classified in three different categories on the basis of their size and confinement. These three types are shortly discussed below.

1.9.2.1 Zero-dimensional nano materials

Nano-materials whose all dimensions are measured in nano scale while no dimension is greater than 100 nm. Mostly, these materials are spherical in nature and have crystalline and amorphous structure. Quantum dots, and gold nanoparticles are zero dimensional nanomaterials.

1.9.2.2 One-dimensional nano-materials

In such type of nano-materials, one dimension of the materials have no nanometer range. These nanomaterials are long up to several micro meters but the diameter of these materials are in a few nanometres, which include nanorods, nanotubes and nanowires etc.

1.9.2.3 Two-dimensional nano materials

Such type of nanostructures have two dimensions are outside the nanometre range. These include mostly nano thin-films such as nano coatings, multilayer sheets, nano wells etc. Nano thin films may be large to several micrometers but their thickness always should be in nanometre range [28].

1.9.3 Nanoparticles

Nano-particles are suggested as the discovery of modern science. The particles whose dimensions are in range up to 100 nm are known as nanoparticles. These particles have potential applications in material science, biomedical, optics and electronic devices. These particles are recently used for filling the voids and pores of superconducting compounds due to their high reactivity and surface to volume ratio. These nanoparticles are classified into magnetic and metallic nano-particles, quantum dots, and metallic oxide nanoparticles etc. For the synthesis of nanostructured materials, different physical and chemical methods are applicable. Physical methods involve subdivision of bulk material, including mechanical crushing. Chemical methods possess decomposition of precursors to form atoms. While two major approaches for the preparation of nanoparticles, include "top to bottom" and "bottom to top" approach. Sol-gel method, micro emulsion method and co-precipitation method are used to synthesize the nanoparticles [29-30].

1.9.4 Applications of Zinc nanoparticles

Zinc (Zn) nanoparticles, nanodots or nano-powder are spherical in shape have more surface. They are metallic in nature and the size of these nanoparticles is typically ranging from 20-100 nanometers (nm) with specific surface area (SSA) in 30 - 50 m²/g range. Applications

of zinc nanoparticles include as an anti-microbial, anti-biotic and anti-fungal (fungicide) agent when incorporated in coatings, bandages, nanofiber, nanowire, plastics, alloy textiles and further research for their remarkable electrical, dielectric, magnetic, optical, imaging, catalytic, biomedical and bioscience properties. These nano-composites are added to improve the grain boundaries and weak links of superconducting materials. The best-known effect of Zn in cuprates is the rapid suppression of critical temperature " T_c ". The rate of " T_c " suppression has been known to be around 10–15 K/ at. % upon Zn substitution. It has been suggested that this rate can be enhanced to 20 K/ at. % near the hole concentration which was discussed to be due to the "pinning" of the charge stripes by Zn impurities [31]. Recently, in this research, the superconducting parameters of high temperature superconducting materials like critical temperature and critical current density are examined and noticed the variations in these parameters after the inclusion of nano- structures [32].

1.10 References

- [1]. D. Delft, and P. Kes, "The discovery of superconductivity" *Phys. Today* **63**, 38 (2010).
- [2]. M. Boerhaave, "History and significance of the discovery of superconductivity by Kamerlingh Onnes in 1911" *Physica C* **479**, 30 (2012).
- [3]. M. Kao, "Synthesis of Y-Ba-Cu-O superconductors from Y_2O_3 , BaO_2 , and Cu_2O the optional oxygen treatment" *Mater. Lett.* **6**, 33 (1987).
- [4]. A. Bertinotti, "Synthesis and characterization of superconducting single crystals of $HgBa_2Ca_2Cu_3O_{8+\delta}$ " *Physica C* **233**, 231 (1994).
- [5]. H. Ibach, and H. Luth, "Solid-State Physics. An introduction to principles of materials Science" Springer, (2009).
- [6]. V. V. Schmidt, P. Muller, and A. V. Ostinov, "The Physics of Superconductors: Introduction to Fundamentals and Application" Springer-Verlag, Berlin, pp. 188 (1997).
- [7]. M. S. Vijay, "Material Science" Mc Graw-Hill Publishing Company Ltd. 59 (2003).
- [8]. G. J. Park, "Asymmetry in the Critical Surface Current of Type-2 Superconductors" *Phys. Rev. Lett.* **15**, 352 (1965).
- [9]. D. Melo, S. C. M. Randeria, and J. R. Engelbrecht, "Crossover from BCS to Bose superconductivity: Transition temperature and time-dependent Ginzburg-Landau theory" *Phys. Rev. Lett.* **71**, 3202 (1993).
- [10]. M. L. Chu, H. L. Chang, C. Wang, J. Y. Juang, T. M. Uen, and Y. S. Gou, "A Search for a Low Anisotropic Superconductor" *Appl. Phys. Lett.* **59**, 1123 (1991).
- [11]. J. Bardeen, L. N. Cooper, and J. R. Schrieffer, "Theory of superconductivity" *Phys. Rev.* **108**, 1175 (1957).
- [12]. A. K. Saxena. "High-Temperature Superconductors" Springer, Berlin-Heidelberg, 1521 (2012).
- [13]. G. Soerensen, and S. Gygax, "Evaluation of oxygen isotope experiments on Pr-, Ca-, and Zn-substituted $YBa_2Cu_3O_7$ " *Phys. Rev. B* **51**, 11848 (1995).
- [14]. K. J. Leary, H. Loye, S. W. Keller, T. A. Faltens, W. K. Ham, J. N. Michaels, and A. M. Stacy, "Observation of an oxygen isotope effect in $YBa_2Cu_3O_7$ " *Phys. Rev. Lett.* **59**, 1236 (1987).

- [15]. A. C. Bleszynski-Jayich, "Persistent currents in normal metal rings". *Sci.* **326**, 272 (2009).
- [16]. C. C. Torardi, "Crystal structure of $Tl_2Ba_2Ca_2Cu_3O_{10}$, a 125K superconductor" *Science* **240**, 631 (1988).
- [17]. Nawazish. A. Khan, M. Mumtaz, "Absence of pair breaking effect in $Cu_{0.5}Tl_{0.5}Ba_2Ca_2Cu_{3-y}Zn_yO_{10-s}$ ($y= 0, 0.75, 1.5, 2.25, 2.5, 2.65$) superconductor" *The Eur. Phys. J. Appl. Phys.* **38**, 47 (2007).
- [18]. M. Hervieu, " $Tl_2Ba_2Ca_3Cu_4O_{12}$, A new 104 K superconductor of the family $(AO)_3(A'CuO_{3-y})_m$ " *Modern Phys. Lett. B* **2**, 1103 (1988).
- [19]. K. C. Goretta, J. G. Chen, N. Chen, M. C. Hash, and D. Shi. "Synthesis of TI-Ca-Ba-Cu-O superconductors" *Mat. Res. Bull.* **25**, 791 (1990).
- [20]. W. J. Stark, L. Mädler, M. Maciejewski, S. E. Pratsinis, and A. Baiker, "Flame-synthesis of Nanocrystalline Ceria/Zirconia: Effect of Carrier Liquid" *Chem. Commun.* 588 (2003).
- [21]. M. J. Bowick, D. R. Nelson, and A. Travesset, "Interacting topological defects on frozen topographies." *Phys. Rev. B* **62**, 8738 (2000).
- [22]. W. D. Callister, and D. G. Rethwisch, "Materials science and engineering: an introduction" vol 7, New York: Wiley, (2007).
- [23]. A. Morawiec, "Tilt and twist grain boundaries" *J. Appl. Crystallograp.* **42**, 308311 (2009).
- [24]. D. A. Molodov, V. A. Ivanov, and G. Gottstein, "Low angle tilt boundary migration coupled to shear deformation" *Acta mater.* **55**, 1843 (2007).
- [25]. D. Dew-Hughes, "The role of grain boundaries in determining J_c in high-field high-current superconductors" *Philoso. Magaz. B* **55**, 459 (1987).
- [26]. G. Cao, "Nano Structures & Nanomaterials" Imperial College Press, London (2004).
- [27]. C. Buzea, I. I. P. Blandino, and K. Robbie, "Nanomaterials and Nanoparticles Sources and Toxicity" *Biointerphases* **2**, 17 (2007).
- [28]. A. Alagarasi, "Introduction to Nanomaterials" Narosa Publishing House, Kolkata (2009).
- [29]. S. R. Foltyn, "Materials science challenges for high-temperature superconducting wire" *Nat. mater.* **6**, 631 (2007).
- [30]. X. Q. Wang, and A. S. Mujumdar. "Heat transfer characteristics of nanofluids: a review" *Int. J. therm. Sci.* **46**, 1 (2007).
- [31]. Y. Hanaki, Y. Ando, S. Ono and J. Takeya, "Zn-doping effect on the magnetotransport properties of $Bi_2Sr_{2-x}La_xCuO_{6+s}$ single crystals" *Phys. Rev. B* **64**, 172514 (2001).

[32]. G. Liu, X. Zhang, Y. Xu, X. Niu, L. Zheng, X. Ding, "The preparation of Zn²⁺-doped TiO₂ nanoparticles by sol-gel and solid phase reaction methods respectively and their photocatalytic activities" *Chemosphere* **59**, 1367 (2005).

Chapter 2

Literature Review

Polycrystalline material of $\text{Sr}_{14}(\text{Cu}_{1-y}\text{M}_y)_{24}\text{O}_{41}$ ($\text{M}=\text{Zn}, \text{Ni}$) was synthesized by using ordinary solid-state reaction technique. No transformation of lattice parameters a , b , c was observed in the sample up to $y=0.05$. The Zn and Ni impurity in the sample reduced the electrical resistivity and slightly enhance the carrier transport property but still the compound was at semi conductive phase. In order to decrease the electrical resistivity, Zn doping played better role than Ni on host polycrystalline matrix. The fitting result proved the conduction mechanism above cross over temperature " T_p " was due to thermal-activated single-holes existence, and below " T_p " one-dimensional hopping conduction was dominated [1].

The single crystal structure of YBaCu_3O_7 was prepared for thin film fabrication [2]. The current density of crystalline structure was less than single crystal structure. Similarly, the surface defects like grain-boundaries and wrinkles were reduced in crystalline structure. Another result revealed that the current density and superconducting transport properties were enhanced by using solid-state reaction. The reduction in grain boundaries was examined in thin film by diffusion due to which J_c remained 103 A/cm^2 for 77 K. But for particular position, J_c approached its maximum value i.e. $106 < J_c < 107 \text{ A/cm}^2$ at a temperature of 77 K. This concluded that the preparation of single superconducting phase of YBaCu_3O_7 was much difficult task.

$(\text{BaO}, \text{CaO}_2 \text{ and CuO})_y/\text{CuTi-1223}$ nanoparticles superconducting composite was synthesized [3]. The scanning electron microscopy images show the improvement in the intergranular links among the superconducting grains with increasing nanoparticles concentration. Microcracks were healed up with the inclusion of these nanoparticles which superconducting volume fraction. The dielectric properties of these composites strongly depend upon the frequency and temperature. The zero resistivity, critical temperature and dielectric properties showed opposite trend with the addition of nanoparticles in $\text{Cu}_{0.5}\text{Tl}_{0.5}\text{Ba}_2\text{Ca}_2\text{Cu}_3\text{O}_{10-\delta}$ superconductor matrix.

$\text{YBa}_2\text{Cu}_{3-x}\text{M}_x\text{O}_{7-y}$ Superconducting phase was prepared for the investigation of physical properties [4]. The suppression of " T_c " for both nonmagnetic and magnetic behavior was observed. For 40 K, " T_c " was suppressed with increasing doping concentration, whether the doping ion is magnetic (Co, Fe, or Ni) or diamagnetic (Al or Zn). This suggested that the behavior of these materials with respect to magnetic impurities was different than conventional Bardeen-Cooper-Schrieffer (BCS)-type superconductors. This might be related to the

uncommon anisotropic oxide structure of these compounds or to the fact that they may not be conventional BCS-type superconductors.

The effect of Ag nanoparticles was observed for the critical current of $\text{YBa}_2\text{Cu}_3\text{O}_{7-\delta}$ (YBCO) superconductor. Alcohol solution was used for the fabrication of Ag nanoparticles while solids state reaction was used for synthesizing the superconducting sample. SEM images revealed that the inter-grain coupling effect and crystallization were improved in the bulk of YBCO superconducting sample with the addition of Ag nanoparticles. Also by increasing the particle size of silver nanoparticles up to 700 nm, the J_c values increased monotonically but decreased by further increasing Ag particles size. The critical current enhancement attributed to the improved connectivity between the grain-boundaries and better crystallization of the grains [5].

$(\text{Cu}_{0.5}\text{Tl}_{0.25}\text{Pb}_{0.25})\text{Ba}_2\text{Ca}_2\text{Cu}_3\text{O}_{10-\delta}$ superconducting matrix was synthesized to observe the physical properties with the addition of ZnO nanoparticles [6]. Co-precipitation method was used for ZnO nanoparticles while solid state reaction method for the preparation of $(\text{Cu}_{0.5}\text{Tl}_{0.25}\text{Pb}_{0.25})$ -1223 superconducting sample. ZnO nanoparticles were mixed with host superconducting matrix in appropriate wt. %. Different concentrations of ZnO nanoparticles ($x=0.0, 0.4, 0.8, 1.2$ wt. %) were added in superconducting matrix. The high concentration ($y > 0.8$) of nano-ZnO increased the secondary phases and enhanced the grain-boundary resistance. This was due to high concentration of nano-ZnO addition, which induced large agglomeration between the superconducting grains. The superconducting transition temperature for $(\text{Cu}_{0.5}\text{Tl}_{0.25}\text{Pb}_{0.25})$ -1223 was found to be lower than that of $(\text{Cu}_{0.5}\text{Tl}_{0.5})$ -1223. This was probably due to the presence of Pb in the charge-reservoir layer increases carriers concentration. This led to stop the flow of mobile carriers to the conducting CuO_2 -planes and hence reduced superconducting transition temperature.

NiO_2 nanoparticles were added for flux pinning and phase formation of $(\text{Bi}_{1.8}\text{Pb}_{0.4}\text{Sr}_2\text{Ca}_{2.2}\text{Cu}_3\text{O}_\delta)_{10-x}(\text{NiO})_x$. Different concentrations like 0.001, 0.002, and 0.003 of NiO_2 nanoparticles were used [7]. Characterizations like XRD (for crystal structure), SEM (for surface morphology), AFM and magnetization measurement were carried out. XRD result showed that the two main phases of Bi-2223 and Bi-2212 were added in bulk of $(\text{Bi}_{1.8}\text{Pb}_{0.4}\text{Sr}_2\text{Ca}_{2.2}\text{Cu}_3\text{O}_\delta)_{10-x}(\text{NiO})_x$. While adding the NiO_2 nanoparticles in the sample, Bi-2212 phase increased its volume fraction while Bi-2223 reduced its volume fraction. For $x=0.002$ concentration of NiO_2 nanoparticles, the flux pinning value increased which implied that the current density " J_c " was enhanced due to the increasing in flux pinning strength. Hence improvement in inter-grain coupling and superconducting transport carriers were achieved.

The effect of nano-SnO₂ addition on the mechanical properties of (Cu_{0.5}Tl_{0.5})-1223 superconducting phase was studied [8]. XRD analysis revealed that the volume fraction of (Cu_{0.5}Tl_{0.5})-1223 phase increased with nano-SnO₂ addition up to 0.6 wt. %, afterwards it showed slight retardation. Although, there was no peaks for SnO₂ or Sn-based compounds appeared in XRD patterns. The EDS results showed the existence of Sn element in the bulk samples. This was evidence that nano-SnO₂ did not enter the structure of the phase. SEM examination clarified that the addition of nano-SnO₂ increased the microstructure density and reduced porosity among the grains. This was also confirmed from the porosity calculations. The microhardness of the studied samples decreased with increasing the applied load up to 1.96 N. The elastic modulus increased with increasing both density and nano-SnO₂ addition, while it decreased with increasing the applied load from 0.49 N to 2.94 N.

The effect of nano-sized MgO (40–60 nm) addition on the physical properties of polycrystalline (Cu_{0.25}Tl_{0.75})-1234 was studied. The MgO-concentration (x) varied from 0 to 1.0 wt. % of the sample's total mass. Phase examination by X-ray diffraction indicated that MgO-addition enhanced the (Cu_{0.25}Tl_{0.75})-1234 phase formation till $x = 0.6$ wt. %. Granular investigation by scanning electron microscope revealed that both number and size of voids decreased as x increased from 0 to 0.6 wt. %. These results were supported by the sample's porosity calculation. However, the addition of a larger amount of MgO > 0.6 wt. % decreased the phase formation, grain connectivity, transport critical current density and microhardness. This decrease was believed to be due to large amount of MgO agglomerated between the grains and hence reduced superconducting grain connectivity and deteriorated intergranular critical current density [9].

The reduction in critical temperature " T_c " of GdBaSrCu₃O_{7- δ} material with addition of Ni and Zn impurities was reported [10]. More concentrations of Ni and Zn impurity content produced the gradual decrease in critical temperature. But the transition width of the sample remained constant for both Ni and Zn impurities. The interruption in spin correlation of the antiferromagnetic CuO₂ planes reduced the critical temperature " T_c ". The suppression of " T_c " for nonmagnetic Zn impurities was significantly more than magnetic Ni impurities. Moreover, if the fact that Zn substituted in Cu(2)-O₂ planes and Ni in Cu(1)-O chains, it could be assumed that probably Cu(2)-O₂ planes may play an important role of superconductivity compared with Cu(1)-O chains.

MgO nano-sized particles were added to Tl_{0.9}Bi_{0.1}Sr_{1.95}Ta_{0.05}Ca_{0.9}Y_{0.1}Cu₂O_{7- δ} superconductor in various weight fraction between 0 to 0.8 wt. % before sintering using the conventional solid state synthesis method [11]. The phase formation and the microstructure of

the samples were studied by XRD and SEM, respectively. The highest critical temperature " T_c " zero of 80 K was observed at 0.2 wt. % MgO and " T_c " was gradually suppressed for higher MgO additions. The effect of the MgO addition on J_c revealed maximum J_c at 0.2 wt. % MgO addition. SEM investigations revealed no difference in microstructure for the pure sample and the MgO added samples. The results showed that a small amount of MgO addition (0.2 wt. %) in Tl-1212 enhanced J_c . The enhanced J_c behavior as a result of MgO addition suggested due to increased magnetic flux pinning of the sample.

Wet chemical method was used to synthesize polycrystalline superconducting phase of $\text{La}_{2-x}\text{Sr}_x\text{Cu}_{1-y}\text{Zn}_y\text{O}_{4-y}$; $y = 0, 0.02$. Strontium concentration was also added with Zn to achieve the better superconducting properties. The principle Bragg peak of the sample was identified by XRD for Zinc concentration [12]. Zero field cooling magnetization and resistivity measurements allowed following the critical temperature as a function of charge carrier concentration. The experimental results obtained were compared to others reported on similar $\text{La}_{2-x}\text{Sr}_x\text{CuO}_{4-\delta}$ samples showing that good quality single-phase polycrystalline samples, with several carrier concentrations, can be obtained using the wet-chemical method. In conclusion, this work confirmed that the wet-chemical method represents an important alternative tool to obtain polycrystalline samples of the $\text{La}_{2-x}\text{Sr}_x\text{Cu}_{1-y}\text{Zn}_y\text{O}_{4-y}$ high- T_c superconductor system having several carrier concentrations, structural instabilities and good quality.

Bulk superconductor samples of type $\text{TlBa}_2\text{Ca}_2(\text{Cu}_{3-x}\text{Co}_x)\text{O}_{9-\delta}$ with $0 \leq x \leq 0.6$ were prepared by a single-step solid-state reaction [13]. The prepared samples characterized by powder X-ray diffraction and the superconductivity of these samples was investigated by electrical resistivity and ac magnetic susceptibility. The depression in the transition temperature could be explained due to Cooper pair breaking mechanism. There was no separation between the inter-grain and the dissipative inter-grain transition in the ac magnetic susceptibility. This observation indicated good electrical contacts between the superconducting grains. The critical current density as well as the reversibility field decreased as Co content increased.

$\text{Bi}_{1.6}\text{Pb}_{0.4}\text{Sr}_{1.9}\text{Ca}_{2.1}\text{Cu}_3\text{O}_{10-\delta}$ Superconducting matrix was synthesized by ordinary solid state reaction [14]. Al_2O_3 nanoparticles of 50 nm were added in that sample for different concentrations (0.0-1.0 wt. %). The addition of a small amount of Al_2O_3 (0.2 wt. %) increased critical current density " J_c " at 77 K by 30% and improved " J_c " behaviour in applied magnetic field either parallel or perpendicular to the sample wide surface (SWS). This results indicated that the introduction of a proper amount of nano- Al_2O_3 particles during the final processing of

BPSCCO samples effectively improved the flux pinning ability and a little detrimental effect on the (Bi, Pb)-2223 formation process.

Superconducting matrix of $Ba_2Ca_{n-1}Cu_nO_{2n} (O, F)_2$ ($n=1, 2, 3, 4, 5$) was synthesized under high pressure [15]. The stoichiometric constituents of $Ba_2Ca_3Cu_4O_8 (O_{1-y+\delta}, F_y)_2$ sample with $y=0.5, 0.6, .7, 0.8$ was synthesized for $n=3, 4$ single phase formation. Superconducting properties changed for magnetic susceptibility and electrical resistivity. Transition temperature enhanced drastically by reducing the fluorine content. The calculated transiting temperature were 90 K, 120 K, 105 K and 90 K against $n=2, 3, 4, 5$ respectively. " T_c " was maximum for $n=3$ but J_c values and irreversibility field decreased for increasing the temperature due to small carrier density.

Zinc ferrite $(ZnFe_2O_4)_y$ nanoparticles/ $Cu_{0.5}Tl_{0.5}Ba_2Ca_2Cu_3O_{10-\delta}$ (CuTl-1223) superconductor composites with $y=0$ to 2 wt. % were prepared by adding $ZnFe_2O_4$ nanoparticles into CuTl-1223 superconductor matrix [16]. The XRD analysis showed that increased concentration of $ZnFe_2O_4$ nanoparticles did not disturb the tetragonal structure of host CuTl-1223 superconductor matrix and has no appreciable effect on its lattice parameters. The SEM images confirmed the granular structure of host superconductor matrix. The presence of $ZnFe_2O_4$ nanoparticles in host superconductor matrix was confirmed by using FTIR study. Variation of zero resistivity critical temperature $\{T_c(0)\}$ depends upon the concentration of the nanoparticles in the host superconductor matrix. The overall suppression of T_c and diamagnetism with increasing nanoparticles concentration was most probably due to trapping of mobile free carriers and reflection of spin charge due to presence of paramagnetic $ZnFe_2O_4$ nanoparticles.

Post annealing experiment in oxygen, nitrogen and air atmosphere was carried out in $Cu_{0.5}Tl_{0.5}Ba_2Ca_2Cu_{3-y}Zn_yO_{10-\delta}$ [17]. The superconducting matrix was grown with $a=3.879 \text{ \AA}$ and $c=14.58 \text{ \AA}$ tetrahedral structure. It was noticed that Zn concentration decreased the c-axis in superconducting matrix. Moreover, Zn impurities enhanced the zero resistivity, critical current, critical temperature and diamagnetism of the compound. Superconducting parameters enhanced as a result of post annealing in open atmosphere. The N_2 and O_2 post annealing in Zn added suppressed the superconducting matrix.

The surface morphology of $Cu_{0.5}Tl_{0.5}Ba_2Ca_3Cu_{4-y}Zn_yO_{12-\delta}$ ($y=0, 1.0, 2.0, 3.0, 3.5$) superconductors was examined with four ZnO_2 adjacent planes. XRD confirmed the tetragonal structure of host superconductors for Zn impurities. This concentration enhanced " T_c ", " J_c ", zero resistivity and diamagnetism of the compound. The critical temperature " T_c " was noticed

TH-16333

as 122 K and the onset temperature of superconductivity was 128 K for $y=3.5$. XRD revealed that increasing the impurities decreased the unit cell volume which enhanced the Fermi vector K_F and effective density of states and superconducting transport properties [18].

2.1 References

- [1]. H. Xie, "Doping effect on electronic transport properties of $\text{Sr}_{14}(\text{Cu}_{1-y}\text{M}_y)_{24}\text{O}_{41}$ ($\text{M} = \text{Zn}, \text{Ni}$)" *Physica B* **381**, 168 (2006).
- [2]. E. D. Specht, C. J. Sparks, and A. G. Dhere, "Effect of oxygen pressure on the orthorhombic-tetragonal transition in the high-temperature superconductor $\text{YBa}_2\text{Cu}_3\text{O}_x$ " *Phys. Rev. B* **37**, 7426 (2001).
- [3]. M. Mumtaz, M. Kamran, K. Nadeem, A. Jabbar, Nawazish. A. Khan, A. Saleem, S. Tajammul Hussain, and M. Kamran "Dielectric properties of $(\text{CuO}, \text{CaO}_2, \text{ and BaO})_y/\text{CuTi-1223}$ composites" *J. Low Temp. Phys./ Fiz. Nizk. Temp.* **39**, 806 (2013).
- [4]. J. M. Tarascon, "Structural and physical properties of the metal (M) substituted $\text{YBa}_2\text{Cu}_{3-x}\text{M}_x\text{O}_{7-y}$ perovskite" *Phys. Rev. B* **37**, 7458 (1988).
- [5]. M. Farbod and M. R. Batvandi, "Doping effect of Ag nanoparticles on critical current of $\text{YBa}_2\text{Cu}_3\text{O}_{7-\delta}$ bulk superconductor" *Physica C* **471**, 112 (2011).
- [6]. M. M. Eloker, R. Awad, A. A. El-Ghany, A. A. Shama and A. A. El-Wanis, "Effect of nano-sized ZnO on the physical properties of $(\text{Cu}_{0.5}\text{Tl}_{0.25}\text{Pb}_{0.25})\text{Ba}_2\text{Ca}_2\text{Cu}_3\text{O}_{10-\delta}$ " *J. Supercond. Nov. Magn.* **24**, 1345 (2011).
- [7]. B. A. Albiss, I. M. Obaidat, M. Gharaibeh, H. Ghamlouche and S. M. Obeidat, "Impact of addition of magnetic nanoparticles on vortex pinning and microstructure properties of Bi-Sr-Ca-Cu-O superconductor" *Solid Stat. Commun.* **150**, 1542 (2010).
- [8]. N. H. Mohammad, A. I. Abou-Aly, I. H. Ibrahim, R. Awad and M. Rkaby, "Mechanical properties of $(\text{Cu}_{0.5}\text{Tl}_{0.5})\text{-1223}$ added by nano- SnO_2 " *J. Alloys Compd.* **486**, 733 (2009).
- [9]. R. Awad, "Study of the Influence of MgO nano-oxide addition on the electrical and mechanical properties of $(\text{Cu}_{0.25}\text{Tl}_{0.75})\text{-1234}$ superconducting phase" *J. Supercond. Nov. Magn.* **21**, 461 (2008).
- [10]. T. V. Chang, S. Kambe, and O. Ishii "The study on Zn and Ni substituted $\text{GdBaSrCu}_3\text{O}_{7-\delta}$ superconductor" *physica C* **468**, 1214 (2008).
- [11]. Z. Salleh and A. K. Yahya, "Effect of nano sized MgO particles addition on formation and superconductivity of $\text{Tl}_{0.9}\text{Bi}_{0.1}\text{Sr}_{1.95}\text{Ta}_{0.05}\text{Ca}_{0.9}\text{Y}_{0.1}\text{Cu}_2\text{O}_{7-\delta}$ ceramics" *Solid Stat. Sci. Technol.* **14**, 81 (2006).

- [12]. A. Loose, J. L. Gonzalez, F. Vieira, E. M. Adalopez, B. Saitovitch, and H. A. Borges "Structural characterization of $\text{La}_{2-x}\text{Sr}_x\text{Cu}_{1-y}\text{Zn}_y\text{O}_{4-\delta}$ ($y=0, 0.02$) samples prepared by the wet-chemical method" *J. Alloys Compd.* **474**, 391 (2009).
- [13]. S. Isber, R. Awad, A. I. Abou-Aly, M. Tabbal and J. M. Kaouar "Electric resistivity and magnetic susceptibility studies of Tl-1223 substituted by cobalt" *Supercond. Sci. Technol.* **18**, 311 (2005).
- [14]. M. Annabi, A. M. Chirgui, F. B. Azzouz, M. Zouaoui, and M. B. Salem, "Addition of nanometer Al_2O_3 during the final processing of (Bi, Pb)-2223 superconductors" *Physica C* **405**, 25 (2004).
- [15]. A. Iyo, Y. Tanaka, M. Tokumoto and H. Ihara, "High-pressure synthesis and properties of $\text{Ba}_2\text{Ca}_{n-1}\text{Cu}_n\text{O}_{2n}(\text{O}, \text{F})_2$ ($n=2-5$) superconductors" *Physica C* **366**, 43 (2001).
- [16]. M. Mumtaz, S. Naeem, K. Nadeem, F. Naeem, A. Jabbar, Y. R. Zheng, Nawazish. A. Khan and M. Imran, "Study of nano-sized $(\text{ZnFe}_2\text{O}_4)_y$ particles/ CuTl-1223 superconductor composites" *Solid Stat. Sci.* **22**, 21 (2013).
- [17]. Nawazish A. Khan, and M. Mumtaz, "Absence of pair breaking effect in $\text{Cu}_{0.5}\text{Tl}_{0.5}\text{Ba}_2\text{Ca}_2\text{Cu}_{3-y}\text{Zn}_y\text{O}_{10-\delta}$ ($y=0, 0.75, 1.5, 2.25, 2.5, 2.65$) superconductor" *Eur. Phys. J. appl. Phys.* **38**, 47 (2007).
- [18]. Nawazish A. Khan, and M. Mumtaz, " $\text{Cu}_{0.5}\text{Tl}_{0.5}\text{Ba}_2\text{Ca}_3\text{Cu}_{4-y}\text{Zn}_y\text{O}_{12-\delta}$ ($y=0, 1.0, 2.0, 3.0, 3.5$): Superconductor with four ZnO_2 Planes" *J. Low. Temp. Phys.* **149**, 97 (2007).

Chapter 3

Experimental techniques

3.1 Synthesis of high temperature of superconductors

Superconductors are synthesized in different phases but the single phase formation and the structural homogeneity are still a problem to produce high temperature superconductors. Similarly, the addition of some impurities which corrode the surface regularity are also the basic issues of high temperature superconductor's. Moreover, superconducting coherence length for the dimensions of crystal structure and the degrees of freedom restricted the synthesis of these compounds. Chemical precipitation techniques, solid-state reaction methods and wet sol-gel techniques are famous for fabrication of these materials. Solid-state reaction technique is advised for the synthesis of HTSCs due to its simplicity and most common uses. [1-2].

3.2 Synthesis of $\text{Cu}_{0.5}\text{Tl}_{0.5}\text{Ba}_2\text{Ca}_3\text{Cu}_4\text{O}_{10-\delta}$ precursors

High temperature superconducting material of $\text{Cu}_{0.5}\text{Tl}_{0.5}\text{Ba}_2\text{Ca}_3\text{Cu}_4\text{O}_{12-\delta}$ was synthesized with solid state reaction technique. $\text{Ba}(\text{NO}_3)_2$, $\text{Ca}(\text{NO}_3)_2$ and $\text{Cu}(\text{CN})$ were mixed in appropriate amounts and ground for 2 hours. After grinding, the mixed powder was placed in quartz mortar and then fired in chamber furnace at 880°C for 24 hours. The composite is cooled down to room temperature and ground again for one hour in agate mortar and pastel for homogenous structure. The ground precursor $\text{Cu}_{0.5}\text{Ba}_2\text{Ca}_3\text{Cu}_4\text{O}_{12-\delta}$ was placed again in pre-heated chamber furnace at 880°C for 24 hours. The flow chart of this process of fabrication of precursor is given in Fig. 3.1.

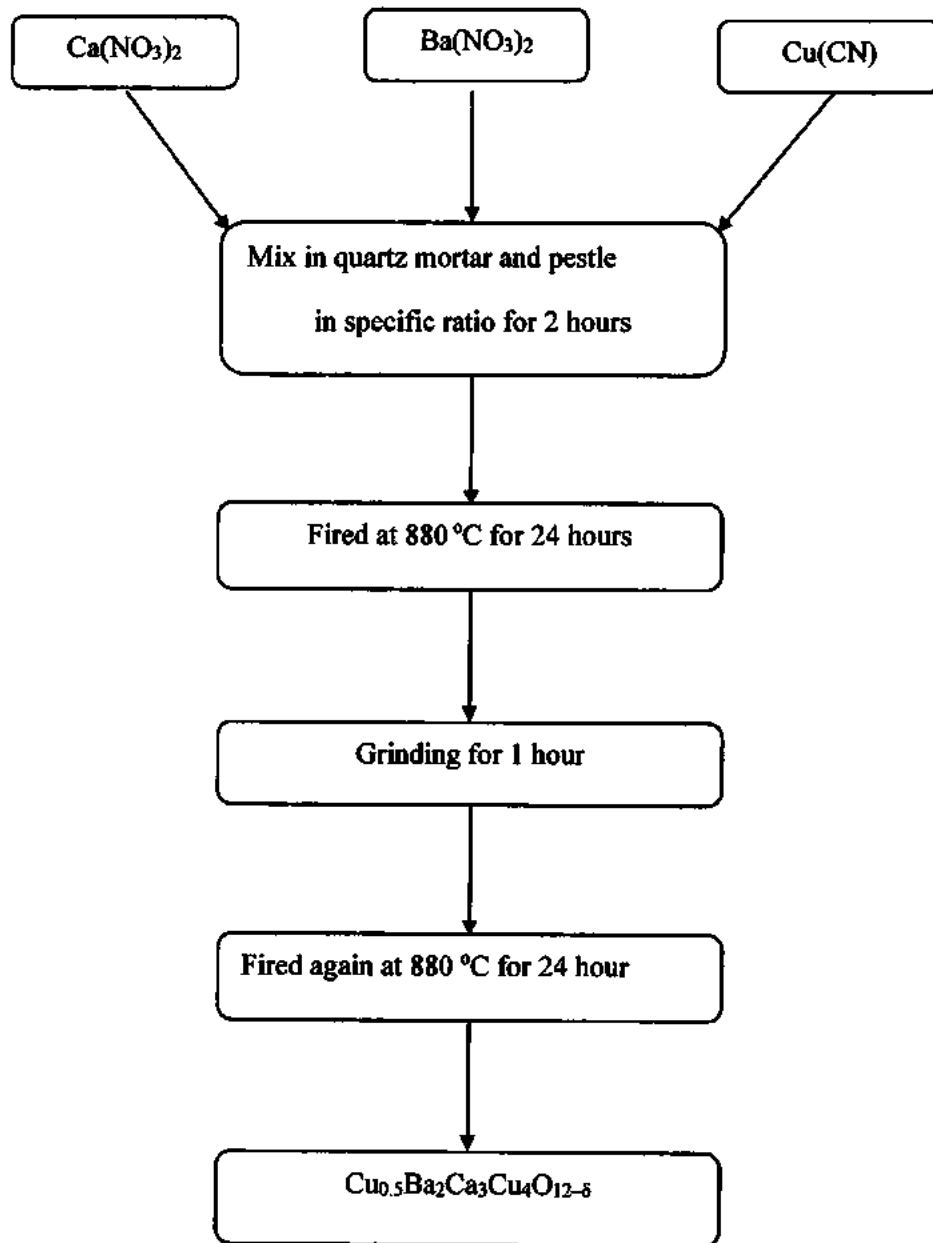


Fig. 3.1: Flow chart for synthesis of $\text{Cu}_{0.5}\text{Ba}_2\text{Ca}_3\text{Cu}_4\text{O}_{12-\delta}$ precursor.

3.3 Methods to synthesize nano-structured materials

Nano structured materials can be synthesized by both chemical and physical techniques. The bulk material is crushed in the presence of high applied voltage for fabrication of metal nano particles. This is simply physical method while in chemical method, the small sized nanoparticles are produced during the reduction of metal ions. Co-precipitation method, precursor decomposition method [3], micro-emulsion method [4] and sol-gel method [5] are

famous chemical methods. The physical method included milling and crushing of bulk materials and sub-division method. But the sol-gel method is considered as best technique to synthesize the suitable nanoparticles in controlled manner.

3.4 Sol-gel technique

Sol-gel technique is very rapid and synthesize the desired nanoparticles in uniform shape and size [6]. This method is very cost effective and highly crystalline for homogenous particles. We can synthesize glass materials and ceramics of thin films, fibers and powders by using sol-gel method. A sol (for solution) is a colloidal or random phase and so small that gravitational force is ignored but only the van der Waals forces and surface charges are present. The gel is the continuous joining networks of particles or ions of semi-rigid mass which are formed after evaporation of the particles as shown in Fig.3.2. Therefore, the sol-gel technique is integrated network (gel) of the colloidal particles of nano-scale which are produced by wet chemical solution. During wet chemical process, the liquid phase is removed and thermal treatment (calcination) is used in favor of polycondensation and for the enhancement mechanical properties of the required gel [7].

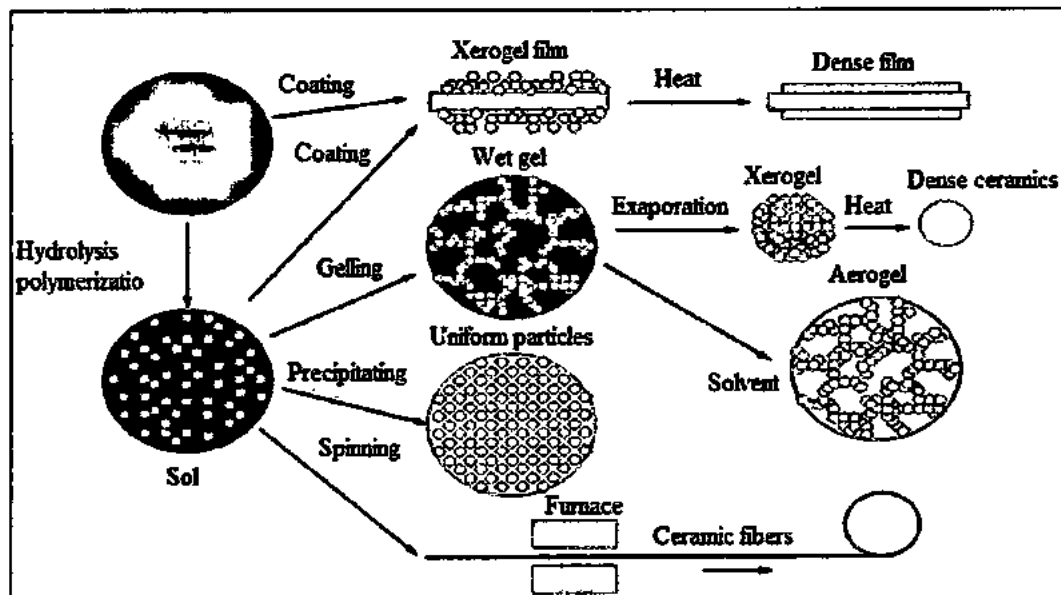


Fig. 3.2: Schematic diagram of Sol-gel process.

3.5 Steps to synthesize Zn added $\text{Cu}_{0.5}\text{Tl}_{0.5}\text{Ba}_2\text{Ca}_3\text{Cu}_4\text{O}_{12-\delta}$ precursor

Two basic steps are included to synthesize $\text{Cu}_{0.5}\text{Tl}_{0.5}\text{Ba}_2\text{Ca}_3\text{Cu}_4\text{O}_{12-\delta}$ precursor with Zn impurities.

After synthesis of Zn nanoparticles and $\text{Cu}_{0.5}\text{Ba}_2\text{Ca}_3\text{Cu}_4\text{O}_{12-\delta}$ precursor, calculated amount (wt.%) of Zn nanoparticles and Tl_2O_3 were added in $\text{Cu}_{0.5}\text{Ba}_2\text{Ca}_3\text{Cu}_4\text{O}_{12-\delta}$ precursor, pelletized, wrapped in gold capsules, sintered at 880°C and got $(\text{Zn})_x/\text{CuTl-1234}$ nano-superconductor composite. The flow chart of whole process is shown in Fig. 3.3.

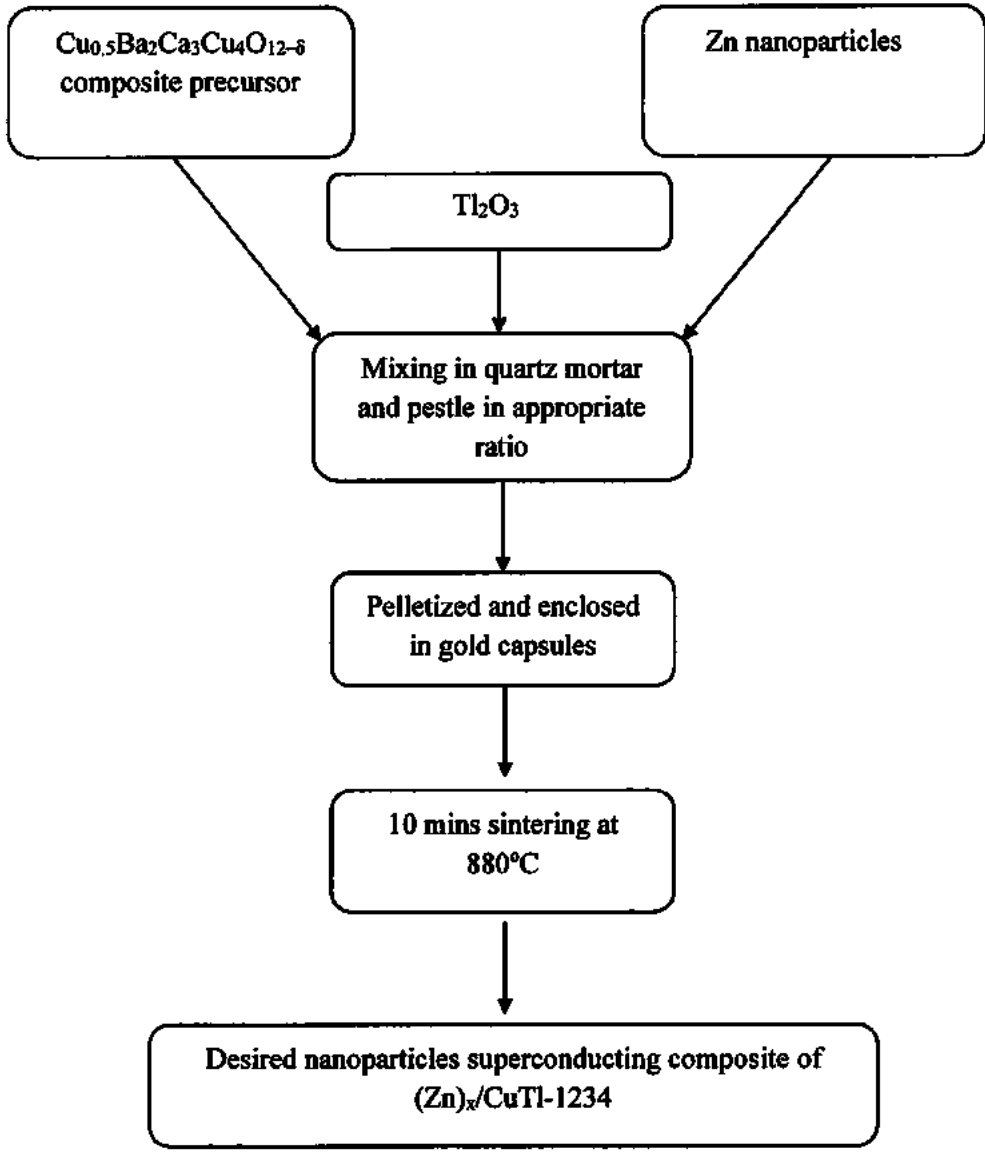


Fig. 3.3: Schematic flow chart of synthesis of Zn nanoparticles/CuTl-1234 nanoparticles superconductor composites.

3.6 Characterization technique

Following techniques were taken out to characterize the synthesized material.

- (1) X-Ray diffraction (XRD) techniques
- (2) Scanning electron microscopy (SEM)
- (3) Fourier transform infrared (FTIR) spectroscopy
- (4) Resistivity verses temperature measurements

3.6.1 X-Ray diffraction (XRD) techniques

Diffraction is basically the bending and spreading of X-rays light in geometrical shadow. To observe diffraction pattern, the width of the slit must be comparable to the wavelength of X-ray light. No diffraction pattern will be observed for either large slit.

3.6.2 X-Ray diffraction in material science

The investigation of material's structure is very important in material science and engineering. The practical application of the materials are not possible without their structural properties. XRD is the finger print of specimen for structural information because it is purely non-destructive technique. Different other information can be obtained by using XRD technique like crystallite size, cell parameters of unit cell and crystalline phases etc. [8]. The inter-planer spacing size of the bulk material and X-ray wavelength must be comparable to each other [9].

3.6.2.1 Bragg's law and X-ray diffraction

In 1914, W. H. Bragg and W. L. Bragg investigated the crystal structure of the solid state material using X-ray diffraction technique. The short wavelength X-rays were carried out for structural investigation of the material. Such type of X-rays are produced by the transition of electron in K-shell as compared to the transitions in L and M-shell [10]. When X-rays fall upon the surface of crystalline materials, some part of these rays are scattered in different directions, diffracted and hit the detector. The detector will detect only those X-rays which have the same phases (constructive interference) while for different phases, no diffraction will occur and hence such waves are not detected by detector (destructive interference).

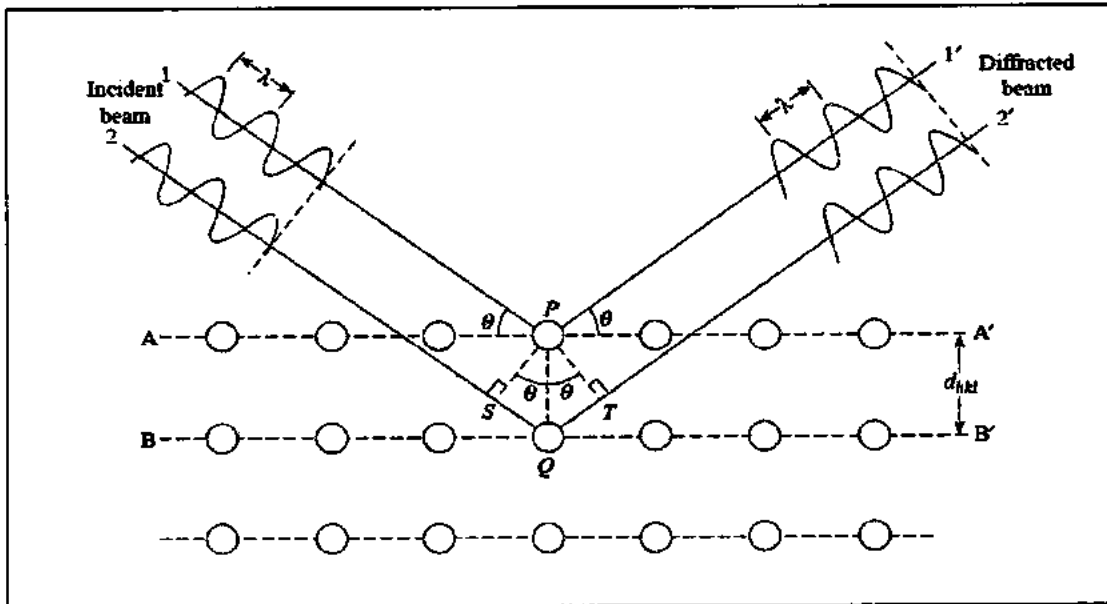


Fig. 3.4: Diffraction of X-rays from crystal planes.

Consider two inter-atomic planes of miller indices (h, k, l) such that they are parallel in direction. Moreover, d_{hkl} is the plane spacing among the given planes. Let X-rays beam of monochromatic source having wavelength λ is incident with angle θ and hit atoms in these parallel planes as shown in Fig.3.4.

If these two rays are in phase with each other then, by constructive interference, they have integral multiple of path difference and strike the detector.

$$n\lambda = 2d \sin \theta \quad 3.1$$

Here "n" represents diffraction order and equation 3.1 is the Bragg's law of diffraction.

The diffraction is occurred for different values of Bragg's angle for constant X-ray wavelength and interplaner spacing. The diffraction pattern is visible only for constructive interference and hence Bragg's law is obeyed but for destructive interference, nothing will be visible on the screen. The Bragg's angle has greater value than 1, so equation 3.1 will be

$$n\lambda / 2d_{hkl} = \sin \theta \quad 3.2$$

Then,

$$n\lambda < 2d_{hkl}$$

For $n=1$, we can write

$$\lambda < 2d_{hkl} \quad 3.3$$

Generally, d_{hkl} is 3 Å or less and hence the X-ray wavelength λ cannot exceed 6 Å [11].

Diffraction also give explanation for the structure of the crystals. These methods are disused as below.

3.6.3 Laue method

In this method, the X-ray source change the wavelength λ while incident angle remain fixed. The experimental set up of Laue method for stationary crystal is shown in Fig.3.5. As the crystal has several number of planes but diffraction is occurred only for the planes where plane spacing "d" and angle " θ " satisfy the Bragg's law.

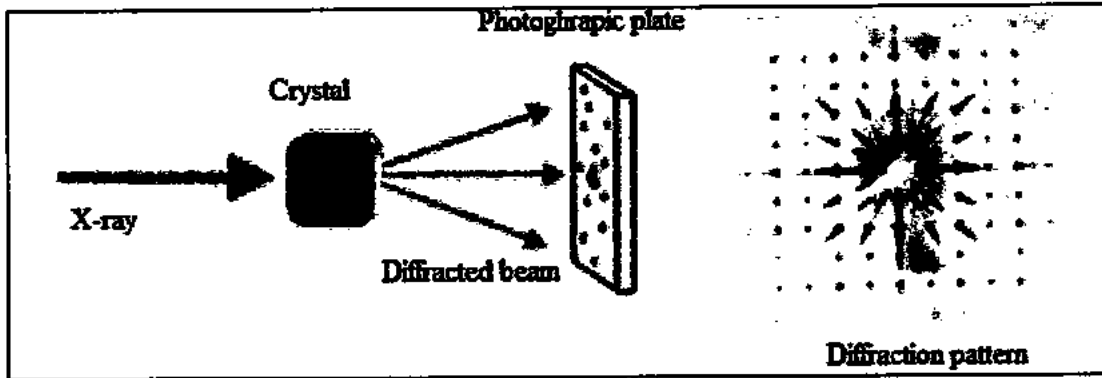


Fig.3.5: Schematic diagram of Laue method.

3.6.4 Rotating crystal method

This method is the reverse of Laue method in which the sample under observation is rotated about an axis of rotation for different angles and the incident X-ray wavelength remains fixed. Again the diffraction pattern is observed only for the angles where X-ray wavelength λ and inter-planer spacing "d" are comparable and enhance the effect of each other as shown in Fig.3.6.

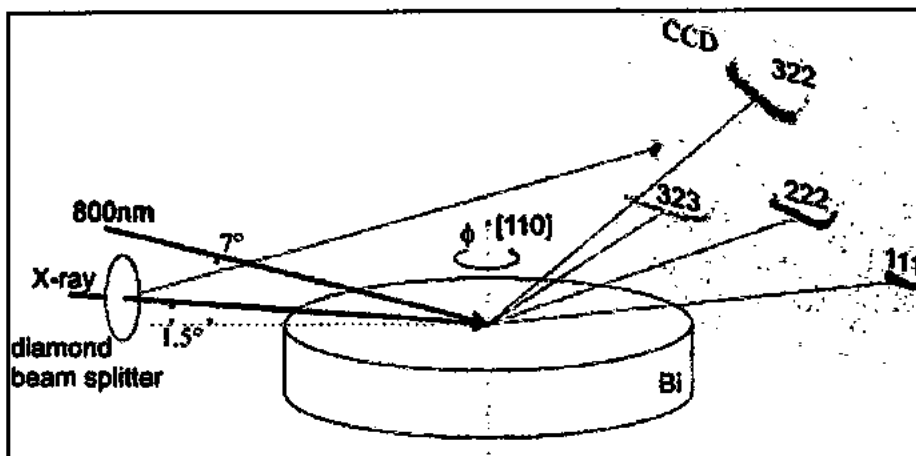


Fig.3.6: Rotating crystal method for fixed X-ray wavelength.

3.6.5 Powder diffraction method

Both spacing "d" and angle "θ" are varied for constant X-ray wavelength "λ" because in this method, the sample is ground in powder form. Again the diffraction is only for that wavelength and angle which satisfy the Bragg's law and Bragg's angle "θ". Powder diffraction is the finger print for reflection plane spacing and calculation of unit cell dimensions for the sample of unknown structure [12].

3.6.6 Debye Scherrer equation

This equation inter-relates the broadening of a peak in diffraction pattern and the size of crystallite in nano-structured materials. This formula is written as;

$$D = k\lambda/B\cos\theta_B \quad 3.4$$

Where D is diameter or average particle size.

k is the shape factor of approximately constant value 0.91.

λ is X-ray wavelength and B is FWHM (full width at half maxima).

3.7 Scanning electron microscopy (SEM)

This technique is one of the most widely used imaging techniques which uses beam of electrons to study the structural morphology of sample. The images of SEM is magnified at high resolution and hence its result is very easy to interpret. Moreover it is purely surface sensitive technique which give information of the specimen depth up to 10 nm [13].

3.7.1 Background of electron microscopy

In 1924, Louis de-Broglie explained the dual nature of light by combining Einstein mass energy relation and max-Planck quantum photonic concept. According to de-Broglie, the equation of wave particle duality is;

$$\lambda = h / p = h/mv \quad 3.5$$

Where p is the momentum, λ is the wavelength of electron and h is planks constant whose value is 6.63×10^{-34} Js.

When kinetic and potential energy of electron become equal in magnitude then

$$\frac{1}{2} m_0 v^2 = eV \quad 3.6$$

Solving for v and putting in equation 3.5, we can write as

$$\lambda = h/(2m_0eV) (\approx 1.22 / V^{1/2} nm) \quad 3.7$$

As SEM is surface sensitive so it explain the surface morphology of the sample, information about particle thickness, surface defects and grain-boundary voids and pores etc.

3.7.2 Operation

The primary beam of electron is generated by tungsten filament electron gun from 500 eV up to 60 keV and is focused by one or more condenser lenses. This beam is then passed through scanning coils where this beam is scanned and objective lenses produce Lorentz force to hit on the target. The aperture polish the sharpness of this beam and hit on the specific area of the sample. The resulted signal is detected by detector, amplified and modulate the sample by cathode ray oscilloscope CRO as shown in Fig.3.7. The resulted signal can be converted from analogue to digital data. The scanning rate of SEM is 15-20 frames/second while for photography record, it takes 30-60 seconds/frame. This microscopy give the result due to secondary electrons. Some other diffraction and spectroscopic techniques like back scattered electrons, reflective high energy electrons, auger electrons and electron beam induced current also give some information about the sample [14].

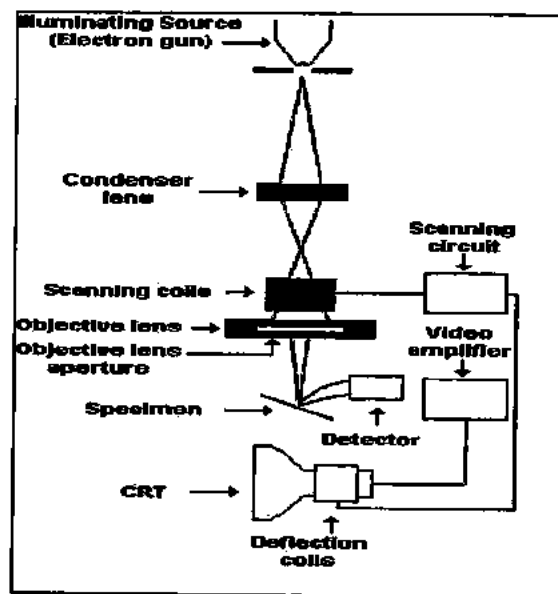


Fig.3.7: Schematic diagram of SEM.

3.7.3 Secondary electron images

SEM is surface sensitive and 95% images are recorded due to secondary electrons because the collection mechanism of these electrons is very easy. Moreover, these electrons are easily controlled because the energy of these electrons is 0-50 eV, much smaller than back

scattered electrons as shown in Fig.3.8. The result of secondary electron depends upon the better adjustment between the contact angle of striking electron beam and sample surface [15].

3.7.4 Back scattered electron images

These are the primary beam electrons within the sample that scattered through an angle approaching 180° . The energy of these electrons is always greater than 50 eV, therefore, it is difficult to detect these electrons on SE detector. The detector of larger area and at a particular direction can detect these electrons. These electrons are the strong source of surface chemistry. Greater the atomic number of the element, greater will be back scattered electrons ejected from the surface of the sample [16].

3.7.5 Auger electrons

When high energetic electrons are incident on the k-shell electron, it is ejected from that shell, as a result, the vacancy is created and vacancy can be filled by neighboring shell electron by releasing an extra energy in the form of photon which is equal to the difference between these two orbits. This photon is sometime hit the outermost electron and this electron is ejected from the atom. This knock out electron is auger electron shown in Fig.3.8 which give us information about the sample structure and compositional analysis of the sample.

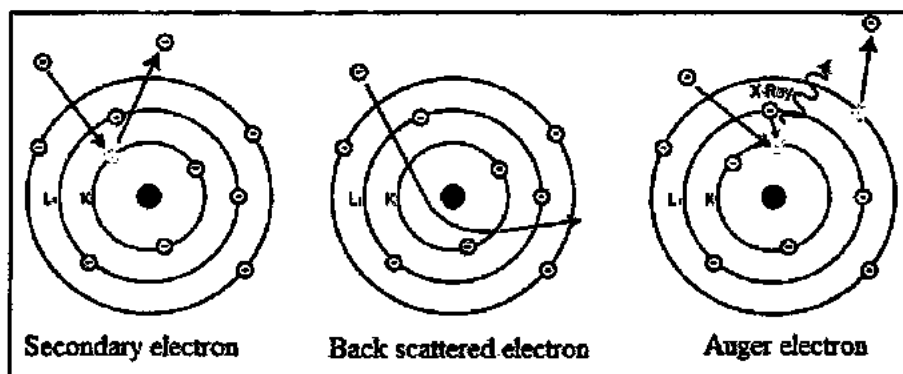


Fig. 3.8: Secondary electron view, backscattered electron and auger electron ejection

3.8 Resistivity measurement

The resistance of a meter cube of the conducting wire is resistivity which depends upon nature of the material and is measured in ohm-meter. The two probe measurement method can measure the resistance in ohm-meter with great accuracy but cannot measure the resistance at lower level like in milli and micro ohm-meter. It is because the contact resistance and lead resistance produce variations in resistivity measurement. The four probe method as shown in

Fig. 3.9 is thus applicable to measure the resistivity at milli and micro level [17]. The normal resistivity and up to certain transition temperature is more interesting phenomenon for high temperature superconductor families.

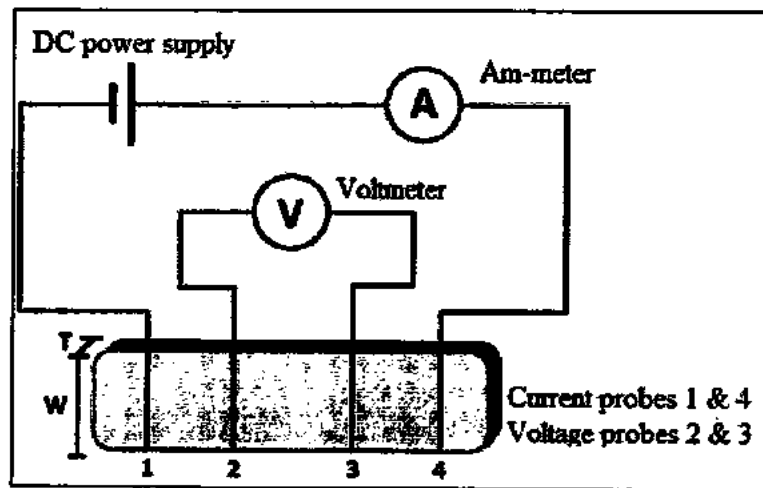


Fig. 3.9: Four-probe technique for resistivity measurement.

3.9 Fourier transform infrared (FTIR) spectroscopy

FTIR spectroscopy gives the information about the sample absorption of infrared light at each wavelength. As each and every atom of the solid exhibit lattice vibrational motion about its mean position. Different materials have different vibrational modes which depend upon the bond length, bond angle and atomic masses of the sample. It is interesting that the atoms also vibrate at 0 K and cannot be controlled [18]. In solid state physics, these lattice vibrations are known as phonons and mathematical expression for phonon energy is

$$E_n = \left(n + \frac{1}{2}\right) \hbar\omega_0 \quad \text{for } n = 0, 1, 2, 3 \dots \quad 3.8$$

For ground state, the above equation will be,

$$E_n = \left(\frac{1}{2}\right) \hbar\omega_0 \quad \text{for } n = 0$$

Here ω_0 represents the frequency of harmonic oscillator and \hbar is the reduced Planck's constant. Lattice vibration is a good technique to determine the vibrational modes present in the sample. Moreover, it explains the physical properties of bulk materials and the phenomenon of FTIR spectroscopy. FTIR spectrometer consists of three fundamental parts which are discussed below.

3.9.1 Michelson interferometer

In this interferometer, two objective mirrors normal to each other are used in which one mirror is stationary while other is moving with $\lambda/4$. The beam splitter is used to divide the incident radiation before striking on the examined sample. Hence beam splitter reflect the infrared light and remaining light is transmitted. The beam splitter is mostly made from potassium bromide on which germanium is coated to split the light in infrared (IR) region. To split the light in far infrared region, thin film of polyethylene terephthalate is used in Michelson interferometer. The transmitted beam of infrared light is perpendicular to incident light beam and detected by FTIR. The moving mirror produced optical path difference, if the path difference is $n\lambda$, constructive interference takes place while for the path difference of $(n+1/2)\lambda$ produce destructive interference [19].

3.9.2 Sources of infrared light

Different sources of infrared light are used for different regions. Tungsten lamp is generally applicable for near infrared region while Nernst source or Glycer light source is used for mid infrared region and mercury based lamp for far infrared region.

3.9.3 Detectors

It is not possible for a single detector to optimize all the desired factors for the entire infrared region as a perfect detector. However, lead sulphide photoconductor is used for near infrared region detector while at liquid helium temperature, germanium detector is operated for far infrared region.

3.9.4 Moving mirrors

Moving mirrors in Michelson interferometer are used to create the path difference between the absorbed and transmitted infrared rays. Interferometer signals recorded by interferogram when the mirror is moving with uniform velocity. Detector transfer this data of infrared region to interferogram. This final infrared spectrum is moved for Fourier transformation where the desired infrared spectrum for intensity verses frequency is displayed. Zero path difference infrared light show larger amplitude of intensity verses frequency graph [20].

3.10 References

- [1]. B. Heeb, S. Oesch, P. Bohac and L. J. Gauckler, "Microstructure of melt-processed $\text{Bi}_2\text{Sr}_2\text{CaCu}_2\text{O}_y$ and reaction mechanisms during post heat treatment" *J. Mater. Res.* **7**, 11 (1992).
- [2]. B. Lehdorff, D. Busch, R. Eujen, and H. Piel, "Preparation and characterization of silver sheathed BSCCO-2223 tapes" *IEEE Trans.* **5**, 2 (1995).
- [3]. N. Millot, S. L. Gallet, D. Aymes, F. Bernard and Y. Grin, "Spark plasma sintering of cobalt ferrite nanopowders prepared by co-precipitation and hydrothermal synthesis" *J. Eur. Ceram. Soc.* **27**, 921 (2007).
- [4]. V. Bartůnek, and O. Smrckova, "Nanoparticles and Superconductors" *J. Ceram. Silik.* **54**, 138 (2010).
- [5]. M. Srivastava, A. K. Ojha, S. Chaubey, P. K. Sharma, and A. C. Pandey, "Influence of pH on structural morphology and magnetic properties of ordered phase cobalt doped lithium ferrites nanoparticles synthesized by sol-gel method" *J. Mater. Sci. Engin. B* **175**, 14 (2010).
- [6]. <http://www.chemat.com/html/solgel.html>.
- [7]. M. A. Hamza, S .K. Asmaa, and M. Y. Hanna. "Synthesis of Yb^{3+} doped TiO_2 nano particles powder as IR filter via sol-gel" *Adv. Mater. Phys. Chem.* **3** (2013).
- [8]. C. Giacovazzo, "Fundamentals of crystallography" Oxford University Press, UK (2002).
- [9]. B. B. He, U. Preckwinkel, and K. L. Smith. "Fundamentals of two-dimensional X-ray diffraction (XRD2)" *Adv. X-ray Anal.* **43**, 273 (2000).
- [10]. B. D. Cullity, "Element of X-ray diffraction" 2nd edition, Addison-Wesely Publishing Company, London, pp. 283 (1977).
- [11]. H. London, "The high-frequency resistance of superconducting tin" *Proceedings of the Royal society of London a mathematical, physical and engineering sciences* Cambridge University Press, (1944).
- [12]. J. Friedel, "Dislocations: International series of monographs on solid state physics" Wesley USA, (2013).
- [13]. B. M. Oliver, and J. M. Cage, "Electronic measurement and instrumentation" McGraw Hill, New York, (1998).
- [14]. S. Bertazzo, E. Gentleman, K. L. Cloyd, A. H. Chester, M. H. Yacoub, and M. M. Stevens, "Nano-analytical electron microscopy reveals fundamental insights into human Cardio-vascular tissue calcification" *Nat. Mater.* **12**, 576 (2013).

- [15]. J. Cazaux, "Mechanisms of charging in electron spectroscopy" *J. Electron. Spectrosc. Relat. Phenom.* **105**, 155 (1999).
- [16]. L. Reimer, "Scanning electron microscopy, Physics of image formation and microanalysis" Springer, (1998).
- [17]. F Gömör, "Characterization of high-temperature superconductors by AC susceptibility measurements" *Supercond. Sci. Technol.* **10**, 523 (1997).
- [18]. P. R. Griffiths, and J. A. D. Haseth, "Fourier transform infrared spectrometry" J. Wiley and Sons, (2007).
- [19]. J. R. Ferraro, and L. J. Basile, "Fourier transform infrared spectroscopy: applications to chemical systems" Academic Press, (1982).
- [20]. M. Gaft, R. Reisfeld and G. Panczer, "Luminescence spectroscopy of minerals and materials" Springer New York, 263 (2005).

Chapter 4

Results and discussions

4.1 Introduction

High temperature superconductors are more effective due to their high superconducting parameters like current density J_c , critical temperature T_c and critical magnetic field H_c . These properties are suppressed due to inter-grain voids and pores which produce inhomogeneous and extra defects that limits the applications and performance of such materials. Superconducting parameters of $\text{Cu}_{0.5}\text{Tl}_{0.5}\text{Ba}_2\text{Ca}_3\text{Cu}_4\text{O}_{12-\delta}$ high temperature cuprate compounds are encouraged for device fabrication because these are prepared at normal pressure but the weak links for inter-grains depress the transport carrier properties of such materials. As a result, these macro surface defects restrict their practical applications. However, these inter-grains empty spaces can be tackled by the inclusion of metallic, non-metallic and magnetic impurities that enhance superconducting parameters and pinning centers to improve the surface morphology. Nanoparticles of different materials due to their high surface to volume ratio and high reactivity can be added in bulk of HTSCs to improve weak-links among the grain boundaries and high critical temperature and current density. Spherical shape metallic Zinc nanoparticles of different concentrations are added in the current study for inter-grain coupling and enhanced scattering cross-section of mobile carriers.

4.2 XRD analysis

X-ray diffraction is very prominent technique to determine the crystal structure of the polycrystalline materials as well as to calculate the polygrained size and atomic arrangement of different unit cells [1]. XRD pattern exhibits prominent diffraction peaks indexed with hexagonal closed pack (HCP) structure of Zn nano-composites as shown in Fig. 4.1. The distinct peaks at 36.34° , 39.06° , 43.28° , 54.36° , 70.1° , 70.68° , and 77.04° diffraction angles correspond to (002), (100), (101), (102), (103), (110) and (004) planes of HCP structure. The HCP structure of Zn nanoparticles matched with the data base of Joint Committee on Powder Diffraction Standards (JCPDS No. 00-004-0784). The size of Zn nanoparticles was

calculated by Debye Sherrer's formula whose average crystallite size was 100 nm.

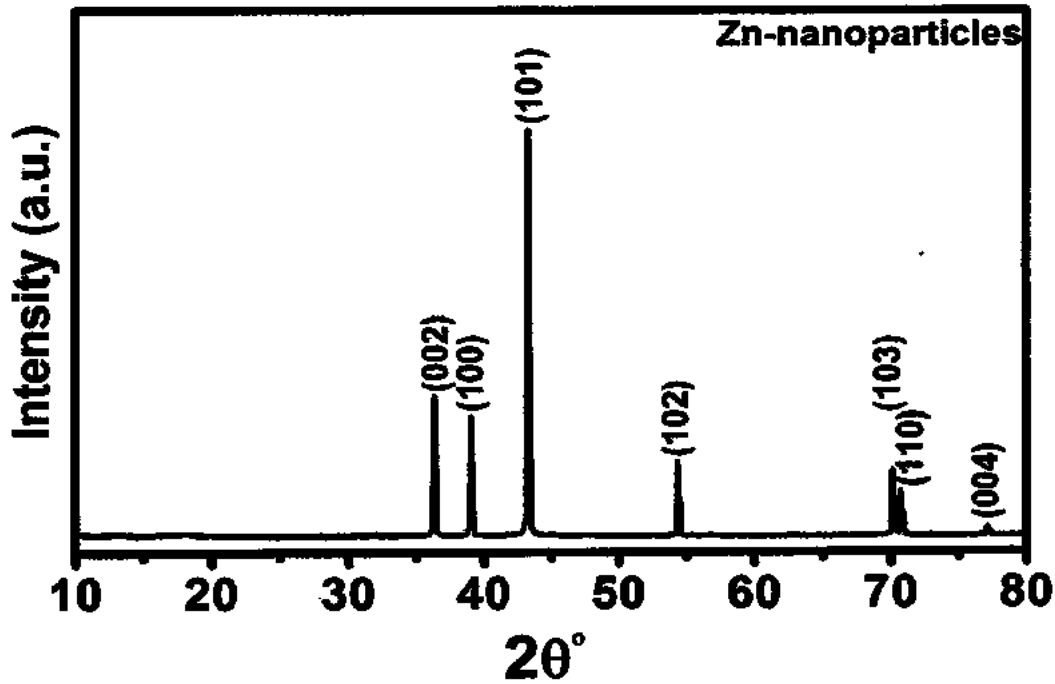


Fig. 4.1: XRD pattern of (Zn) nanoparticles.

XRD patterns of $(\text{Zn})_x/\text{CuTi-1234}$ nanoparticles-superconductor composites with $x = 0 \leq x \leq 3$ wt. % are shown in Fig.4.2. These composites confirmed the tetragonal structure following $P4/mmm$ space group with nearly similar lattice parameters $a = 4.21 \text{ \AA}$ and $c = 18.25 \text{ \AA}$. Mostly diffracted peaks correspond to CuTi-1234 phase. XRD analysis reveals that the Zn nanoparticles inclusion not affected the crystal structure of CuTi-1234 phase. The nonmagnetic Zn nanoparticles of 100 nm in size dispersed themselves on the surface of CuTi-1234 superconductor filled inter-grains weak-links. Small variation in lattice parameters by the addition of Zn nanoparticles in CuTi-1234 superconducting matrix is mainly as a result of oxygen impurities. Some un-indexed peaks of very low intensity observed because of some small other superconducting composite phases. The diffraction peaks were indexed using the computer software MDI-Jade and matched with international center for the diffraction data (ICDD) [2-9].

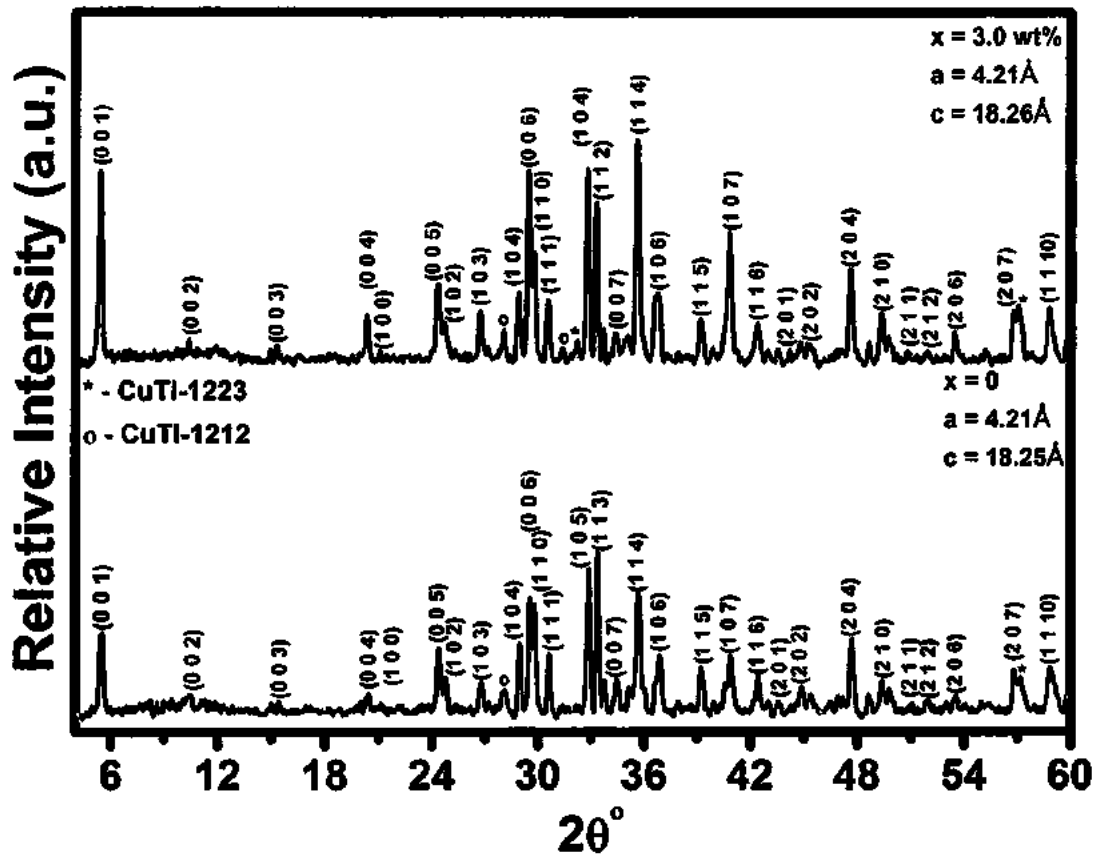


Fig. 4.2: XRD patterns of (Zn)_x/CuTI-1234 superconductors with x = 0.0 and 3.0 wt. %.

4.3 SEM images

This technique is most widely used imaging techniques which uses beam of electrons to study the surface morphology of sample. It is purely surface sensitive technique which gives information about the specimen depth up to 10 nm. SEM micrographs of (Zn)_x/CuTI-1234 (x=0~3 wt. %) nanoparticles-superconductor composites as shown in Fig. 4.3. The enhancement observed in the inter-grains weak-links as well as in grains size after the addition of Zn nanoparticles in CuTI-1234 superconducting matrix [10-13]. The main issue being faced is the non-uniform, inhomogeneous distribution of Zn nanoparticles within entire bulk of CuTI-1234 matrix.

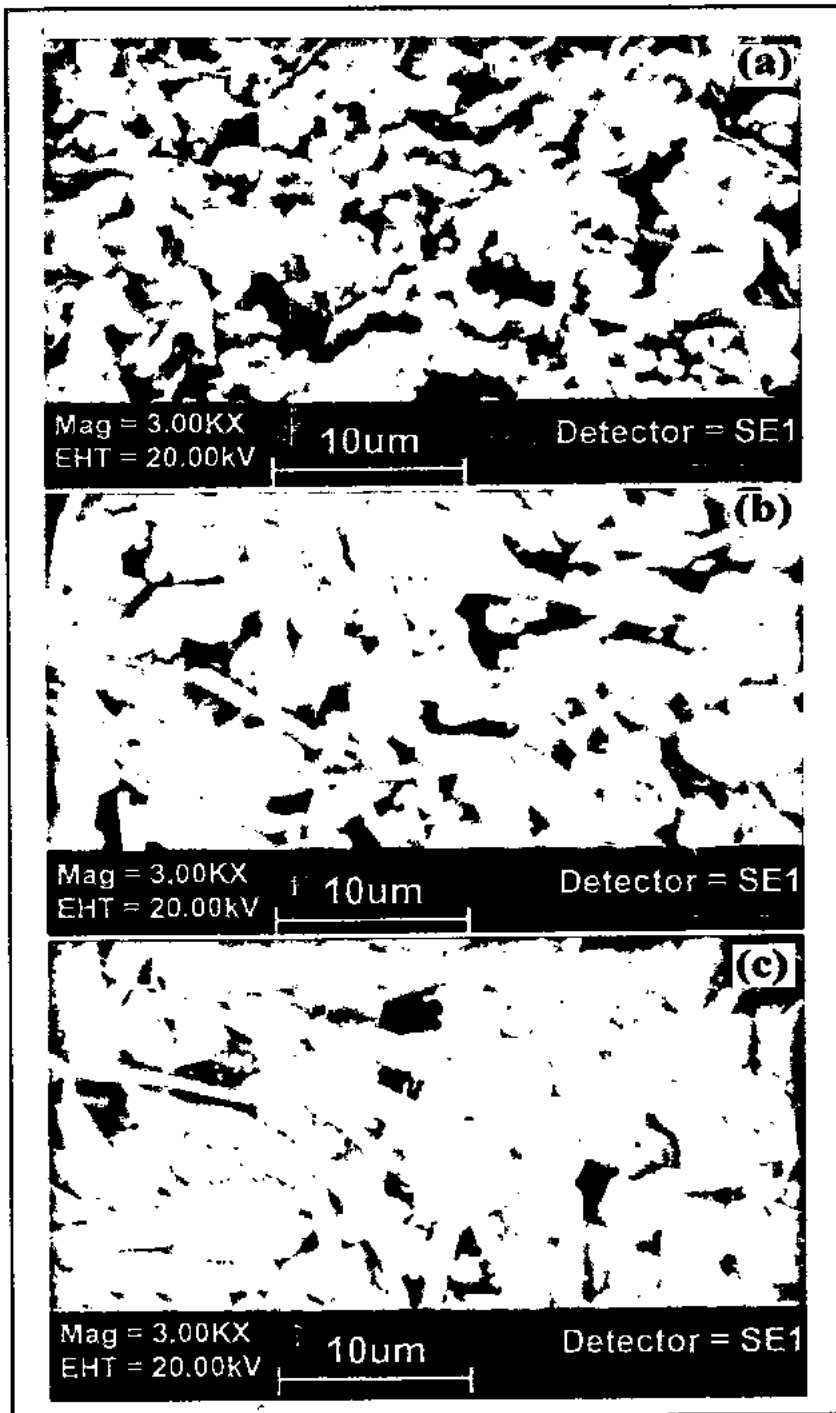


Fig. 4.3: SEMs of (Zn) x /CuTi-1234 composites with (a). $x = 0$, (b). $x = 0.6$ and (c). $x = 1.8$ wt. %.

4.4 FTIR spectroscopy

FTIR absorption spectra of $(\text{Zn})_x/\text{CuTi-1234}$; $x = 0, 0.6, 1.2, 1.8, 2.4$ and 3.0 wt. % nanoparticles-superconductor composites are shown in Fig.4.4. Considering our previous studies to understand the mechanism of superconductivity in HTSC's, the possibility of electron and phonon interaction cannot be ignored. Oxygen related phonon modes are of special interest, since these modes most likely cause such interactions. We have taken FTIR spectra in the range from $400\text{-}700\text{ cm}^{-1}$ in which the bands from 400 to 540 cm^{-1} are associated with the apical oxygen atoms and from 541 to 600 cm^{-1} are associated with CuO_2 planar oxygen atoms. The bands from 670 to 700 cm^{-1} are associated with O_b atoms in the charge reservoir layer [14-17]. But in the pure $\text{Cu}_{0.5}\text{Tl}_{0.5}\text{Ba}_2\text{Ca}_3\text{Cu}_4\text{O}_{12-\delta}$ samples, the apical oxygen modes of type $\text{Tl-O}_A\text{-Cu(2)}$ and $\text{Cu(1)-O}_A\text{-Cu(2)}$ are observed around 415 cm^{-1} and $444\text{-}456\text{ cm}^{-1}$ and CuO_2 planar modes are around 541 cm^{-1} . The apical oxygen mode of type $\text{Tl-O}_A\text{-Cu(2)}$ is slightly hardened to 421 cm^{-1} and $\text{Cu(1)-O}_A\text{-Cu(2)}$ is softened to 518 cm^{-1} in nano-Zn particles added samples, which may be due to stresses and strains produced in the material after the addition of these nanoparticles. Almost the positions of all the oxygen vibrational phonon modes remained unaltered after nano-Zn particles addition in CuTi-1234 matrix. This gives us a clue that Zn did not substitute any atom in the unit cell and remained at the grain-boundaries of $(\text{Zn})_x/\text{CuTi-1234}$ nano-superconductor composites.

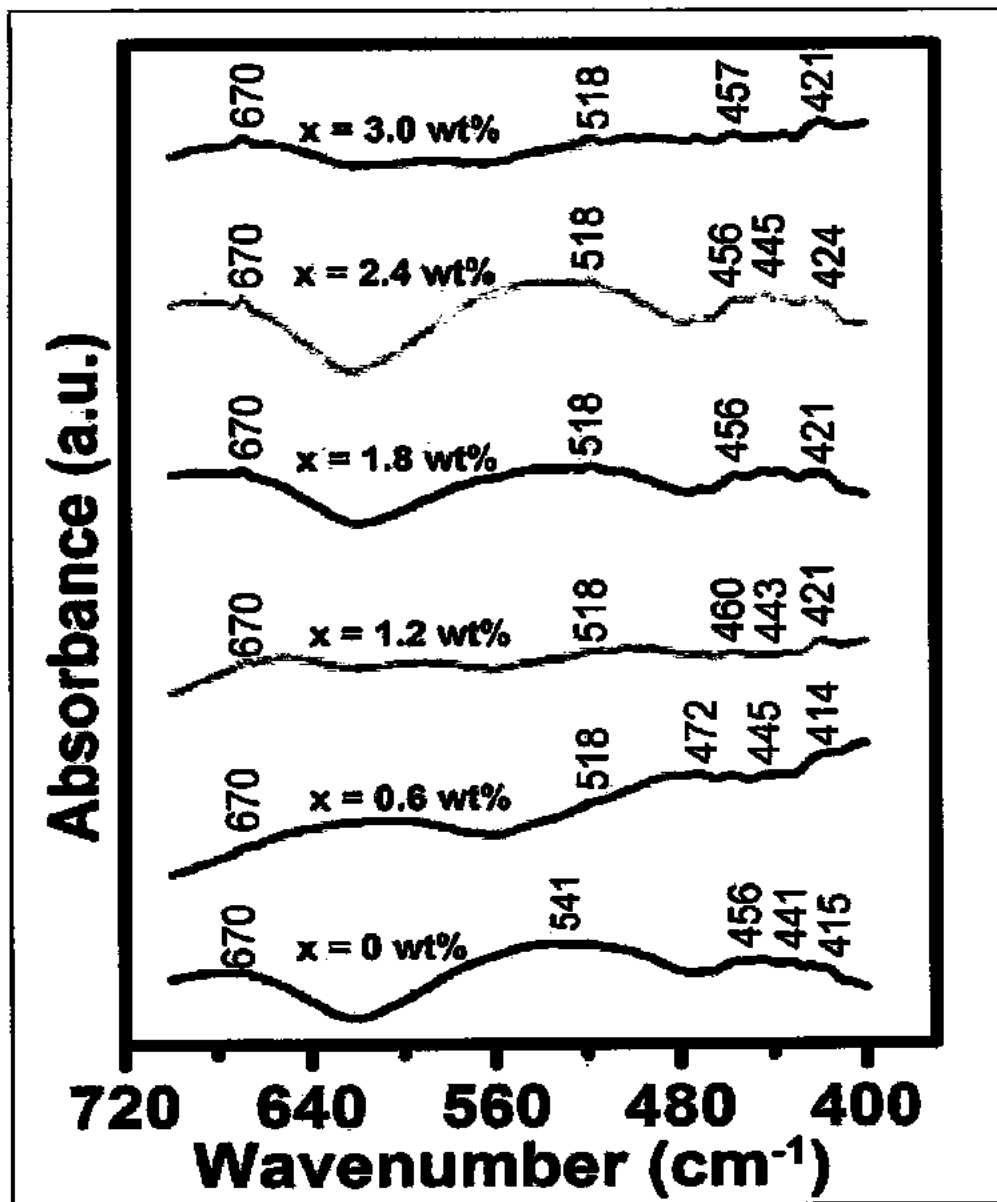


Fig. 4.4: FTIR spectra of $(Zn)_x/CuTi-1234$ composites with $x = 0, 0.6, 1.2, 1.8, 2.4$ and 3.0 wt. %.

4.5 Resistivity measurements

The dc-resistivity versus temperature measurements of $(\text{Zn})_x/\text{CuTi-1234}$; $x = 0, 0.6, 1.2, 1.8, 2.4$ and 3.0 wt. % nanoparticles-superconductor composites are shown in the Fig. 4.5. All the samples exhibit metallic like behavior in variations of dc-resistivity above at superconducting transition temperatures. The four probe method was used for dc-resistivity measurements. Systematic and consistent reduction in T_c values from 105 K for $x = 0$ to 93 K for $x = 3.0$ wt. % was observed. The gradual decrease in T_c with increasing nano-Zn particles content is either due to oxygen vacancy disorder or due to mobile carriers trapping, or due to lesser oxygen content in CuO_2 conducting planes [18-21]. The non-uniform variation in normal state dc-resistivity shows the irregular scattering of carriers across the impurities at the grain-boundaries of CuTi-1234 matrix.

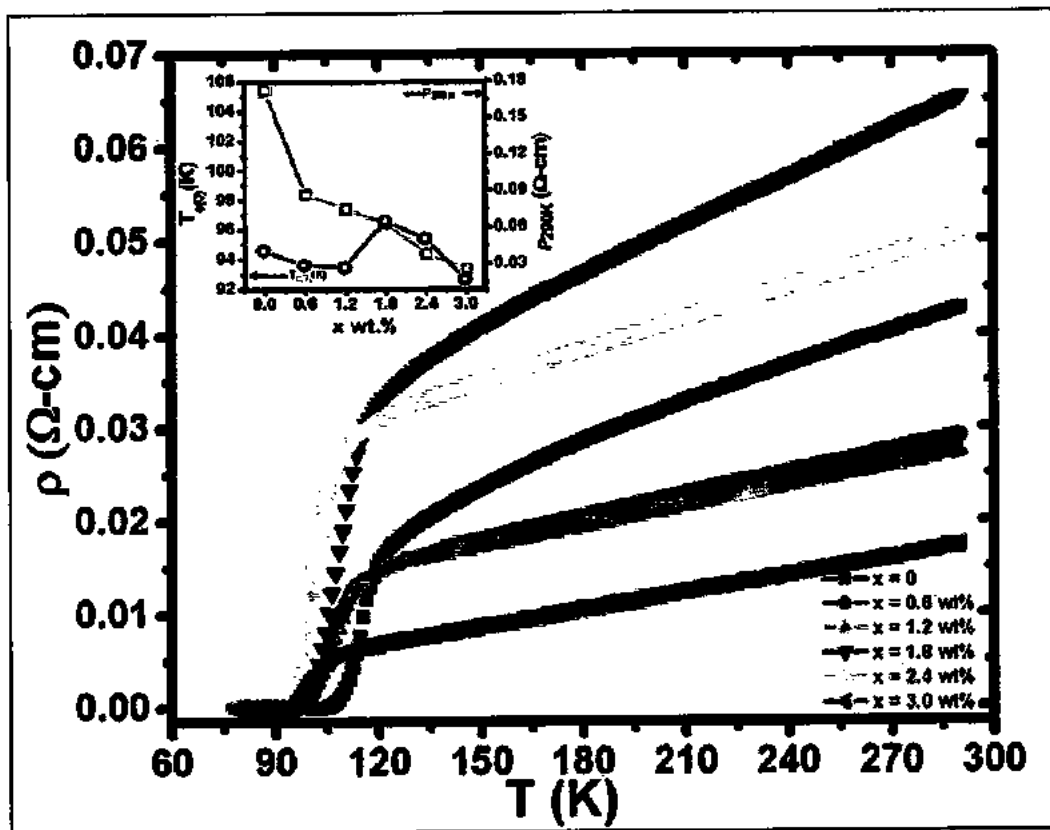


Fig. 4.5: Temperature dependence of resistivity measurements of $(\text{Zn})_x/\text{CuTi-1234}$ composites with $x = 0, 0.6, 1.2, 1.8, 2.4$ and 3.0 wt. %.

4.6 AC-susceptibility measurements

Magnetic ac-susceptibility measurements of $(\text{Zn})_x/\text{CuTi-1234}$ composites are shown in Fig. 4.6. We used SR530 Lock-in amplifier working at frequency of 270 Hz with $H_{AC} = 0.07\text{Oe}$ of primary coil. There is one peak for all samples above the transition temperatures in all ac-susceptibility measurements for different concentrations of nano-Zn particles in CuTi-1234 superconducting matrix. The magnitude of diamagnetism of the superconducting materials is represented by the real part (χ') of the ac-susceptibility and the ac-losses corresponding to the flux penetration in to superconductor samples is represented by imaginary part (χ''). The imaginary part of the ac-susceptibility provides the inter-granular contribution and, therefore, gives information about the nature of inter-grains weak links and pinning strength [22-30]. The suppression of superconductivity within the grains decreases the magnitude of χ' . It is observed that the onset temperature as well as magnitude of diamagnetism has overall been decreased with increased Zn nanoparticles. The peak position in χ'' is clearly shifted to lower temperature values with increased Zn nanoparticles.

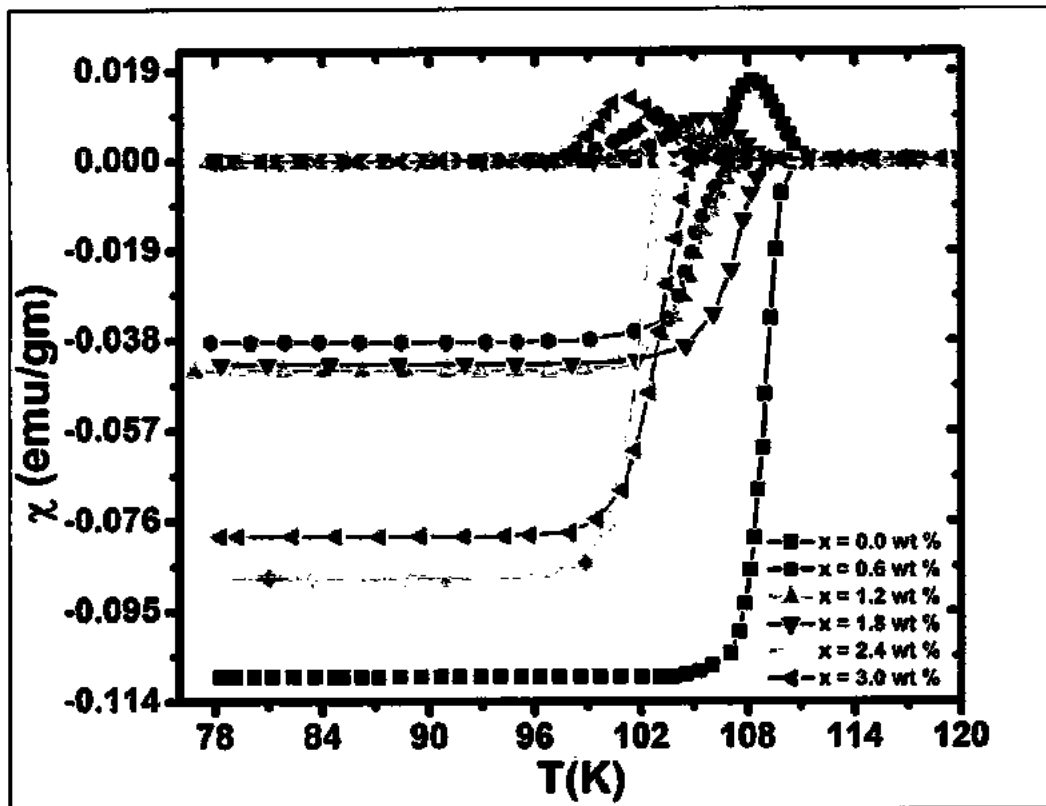


Fig. 4.6: AC susceptibility of $(\text{Zn})_x/\text{CuTi-1234}$ composites with $x = 0, 0.6, 1.2, 1.8, 2.4$ and 3.0 wt. %.

The regular decreasing trend in superconducting properties can be expected due to reduction of superconducting volume fraction with increasing contents of Zn nanoparticles at the grains-boundaries of CuTI-1234 superconductor. The second possible reason may be due to enhanced scattering cross-section of carriers after addition of nanoparticles of nonmagnetic $3d^{10}$ Zn element.

4.7 Conclusion

The effects of Zn nanoparticles addition on superconducting properties as well as phase formation of CuTl-1234 superconductor were studied. We synthesized $(\text{Zn})_x/\text{CuTl-1234}$ composites successfully by well-established solid-state reaction. The tetragonal structure of CuTl-1234 phase was identified by XRD patterns, which remained unaltered and uninterrupted after nano-Zn particles addition. Unaltered crystal structure of host CuTl-1234 phase confirmed the existence of Zn nanoparticles at the inter-crystallite sites. The SEM micrographs have shown the granular structure with enhanced grain sizes after nano-Zn particles addition. The suppression of superconducting properties of CuTl-1234 phase after addition of nonmagnetic of $3d^{10}$ Zn element nanoparticles can be attributed due to reduction of superconducting volume fractions and enhanced scattering cross-section of mobile carriers.

4.8 References

- [1]. C. Giacovazzo, "Fundamentals of crystallography" Oxford University Press, (2002).
- [2]. A. Jabbar, M. Mumtaz, and K. Nadeem, "Noble metals (Ag, Au) nanoparticles addition effects on superconducting properties of CuTl-1223 phase" *Eur. Phys. J. Appl. Phys.* **69**, 7 (2015).
- [3]. A. Jabbar, I. Qasim, K. M. Khan, Z. Ali, K. Nadeem, and M. Mumtaz, "Synthesis and superconducting properties of $(Au)_x/CuTl-1223$ composites" *J. Alloys Compd.* **618**, 110 (2015).
- [4]. Nawazish. A. Khan, A. Saleem, and S. T. Hussain, "Enhanced inter-grain connectivity in nano-particles doped $(Cu_{0.5}Tl_{0.5})Ba_2Ca_2Cu_3O_{10-\delta}$ superconductors" *J. Supercond. Nov. Magn.* **25**, 1725 (2012).
- [5]. G. Hussain, A. Jabbar, I. Qasim, M. Mumtaz, K. Nadeem, M. Zubair, S. Q. Abbas, and A. A. Khurram, "Activation energy and excess conductivity analysis of $(Ag)_x/CuTl-1223$ nanosuperconductor composites" *J. Appl. Phys.* **116**, 103911 (2014).
- [6]. J. M. Tarascon, "Structural and physical properties of the metal (M) substituted $YBa_2Cu_3-xM_xO_{7-y}$ perovskite" *Phys. Rev. B* **37**, 7458 (1988).
- [7]. M. Farbod and M. R. Batvandi, "Doping effect of Ag nanoparticles on critical current of $YBa_2Cu_3O_{7-\delta}$ bulk superconductor" *Physica C* **471**, 112 (2011).
- [8]. M. M. Eloker, R. Awad, A. A. El-Ghany, A. A. Shama and A. A. El-Wanis, "Effect of Nano-Sized ZnO on the Physical Properties of $(Cu_{0.5}Tl_{0.25}Pb_{0.25})Ba_2Ca_2Cu_3O_{10-\delta}$ " *J. Supercond. Nov. Magn.* **24**, 1345 (2011).
- [9]. B. A. Albiss, I. M. Obaidat, M. Gharaibeh, H. Ghamlouche and S. M. Obeidat, "Impact of addition of magnetic nanoparticles on vortex pinning and microstructure properties of Bi-Sr-Ca-Cu-O superconductor" *Solid Stat. Commun.* **150**, 1542 (2010).
- [10]. N. H. Mohammed, A. I. Abou-Aly, R. Awad, I. H. Ibrahim, M. Roumié, and M. Rekaby, "Mechanical and electrical properties of $(Cu_{0.5}Tl_{0.5})-1223$ phase added with nano- Fe_2O_3 " *J. Low Temp. Phys.* **172**, (2013).
- [11]. M. Annabi, A. M. Chirgui, F. B. Azzouz, M. Zouaoui, and M. B. Salem, "Addition of nanometer Al_2O_3 during the final processing of (Bi, Pb)-2223 superconductors" *Physica C* **405**, 25 (2004).

- [12]. A. Ghattas, M. Annabi, M. Zauaoui, F. B. Azzouz, and M. B. Salem, "Flux pinning by Al-based nano particles embedded in polycrystalline (Bi, Pb)-2223 superconductors" *Physica C* **468**, 31 (2008).
- [13]. W. Kong, R. A. Shukor, "Enhanced electrical transport properties of nano NiFe₂O₄-added (Bi_{1.6}Pb_{0.4})Sr₂Ca₂Cu₃O_{10-δ} superconductor" *J. Supercond. Nov. Magn.* **23**, 257 (2010).
- [14]. A. D. Kulkarni, F. W. de Wette, J. Prade, U. Schroder and W. Kress "Lattice dynamics of high-T_c superconductors: Optical modes of the thallium-based compounds" *Phys. Rev. B* **41**, 6409 (1990).
- [15]. M. Mumtaz, Nawazish. A. Khan, and E. U. Khan, "Growth of Cu_{0.5}Tl_{0.5}Ba₂Ca₃Cu_{4y}Zn_yO_{12-δ} (y=0, 1, 1.5, 2, 2.5) superconductor with optimum carriers" *Physica C* **470**, 428 (2010).
- [16]. A. Jabbar, I. Qasim, M. Waqeur-Rehman, M. Zaman, K. Nadeem, and M. Mumtaz, "Structural and superconducting properties of (Al₂O₃)_y/CuTl-1223 composites" *J. Elec. Mater.* **44**, 110 (2015).
- [17]. M. Mumtaz, M. Kamran, K. Nadeem, A. Jabbar, Nawazish. A. Khan, A. Saleem, S. Tajammul Hussain, and M. Kamran "Dielectric properties of (CuO, CaO₂, and BaO)_y/CuTl-1223 composites" *J. Low Temp. Phys./ Fiz. Nizk. Temp.* **39**, 806 (2013).
- [18]. E. Brecht, W. W. Schmahl, G. Miehe, M. Rodewald, H. Fuess, N. H. Andersen, J. Hanbmann, and T. Wolf, "Thermal treatment of YBa₂Cu_{3-x}Al_xO_{6+δ} single crystals in different atmospheres and neutron diffraction study of excess oxygen pinned by the Al substituents" *Physica C* **265**, 53 (1996).
- [19]. P. F. Miceli, J. M. Tarascon, L. H. Greene, H. P. Barbour, F. J. Rotella, and J. D. Jorgensen, "Role of bond lengths in the 90-K superconductor: A neutron powder-diffraction study of YBa₂Cu_{3-x}Co_xO_{7-y}" *Phys. Rev. B* **37**, 5932 (1988).
- [20]. V. P. S. Awana, S. K. Malik, W. B. Yelon, C. A. Cardoso, O. F. de Lima, A. Gupta, A. Sedky, and A. V. Narlikar, "Neutron diffraction on Er_{1-x}Ca_xBa₂Cu₃O_{7-δ} (0.0 ≤ x ≤ 0.3) system: possible oxygen vacancies in Cu-O₂ planes" *Physica C* **338**, 197 (2000).
- [21]. S. Cao, L. Li, F. Liu, W. Li, C. Chi, C. Jing, and J. Zhang, "Structure and charge transfer correlated with oxygen content for Y_{0.8}Ca_{0.2}Ba₂Cu₃O_y (y=6.84–6.32) system: a positron study" *Supercond. Sci. Technol.* **18**, 606 (2005).
- [22]. J. C. Zhang, F. Q. Liu, G. S. Cheng, J. X. Shang, J. Z. Liu, S. X. Cao, and Z. X. Liu, "Electron-structure and vacancy properties and al-substitution dependence of the positron lifetime in y1:2:3 superconducting ceramics" *Phys. Lett. A* **201**, 70 (1995).

- [23]. Y. Hanaki, Y. Ando, S. Ono and J. Takeya, "Zn-doping effect on the magnetotransport properties of $\text{Bi}_2\text{Sr}_{2-x}\text{La}_x\text{CuO}_{6+\delta}$ single crystals" *Phys. Rev. B* **64**, 172514 (2001).
- [24]. T. Kawamata, T. Adachi, T. Noji and Y. Koike, "Giant suppression of superconductivity at $x=0.21$ in the Zn-substituted $\text{La}_{2-x}\text{Sr}_x\text{Cu}_{1-y}\text{Zn}_y\text{O}_4$ single crystals" *Phys. Rev. B* **62**, R11981 (2000).
- [25]. Nawazish. A. Khan, M. Mumtaz, A. A. Khurram and P. Kameli, "AC-susceptibility measurements of $\text{Cu}_{1-x}\text{Tl}_x\text{Ba}_2\text{Ca}_3\text{Cu}_4\text{O}_{12-\delta}$ superconductor thin films with different thallium content" *Physica C* **468**, 233 (2008).
- [26]. R. V. Sarmago, K. L. C. Molina, and L. J. D. Guerra, "A new perspective to AC magnetic susceptibility measurements in an unbalanced mutual inductance bridge" *Physica C* **239**, 364 (2001).
- [27]. H. Xie, N. Hua, L. Wang, Y. Lina, R. Xionga, Z. Yua, W. Tanga, Q. Wang, and J. Shia, "Doping effect on electronic transport properties of $\text{Sr}_{14}(\text{Cu}_{1-y}\text{My})_{24}\text{O}_{41}$ ($M = \text{Zn}, \text{Ni}$)" *Physica B* **381**, 168 (2006).
- [28]. T. Yoshida, "Effects of Zn-impurity scattering in $\text{La}_{2-x}\text{Sr}_x\text{CuO}_4$ studied by angle-resolved photoemission spectroscopy" *Physica C* **460**, 872 (2007).
- [29]. Y. Xu, "Effect of ZrO_2 and ZnO nanoparticles inclusions on superconductive properties of the melt-processed $\text{GdBa}_2\text{Cu}_3\text{O}_{7-\delta}$ bulk superconductor" *Physica C* **468**, 1363 (2008).
- [30]. Nawazish. A. Khan, M. Mumtaz, A. Ullah, N. Hassan, and A. A. Khurram, "Suppression of T_c in Co-doped $(\text{Cu}_{0.5}\text{Tl}_{0.5})\text{Ba}_2\text{Ca}_2\text{Cu}_{3-x}\text{Co}_x\text{O}_{10-\delta}$ superconductor" *J. Alloys Compd.* **507**, 142 (2010).